PHILOSOPHICAL TRANSACTIONS OF THE ROYAL SOCIETY A MATHEMATICAL, PHYSICAL & ENGINEERING SCIENCES

Attenuation in the Earth at Low Frequencies

G. Masters and F. Gilbert

Phil. Trans. R. Soc. Lond. A 1983 **308**, 479-522
doi: 10.1098/rsta.1983.0016

Phil. Trans. R. Soc. Lond. A **308**, 479–522 (1983) [479]
Printed in Great Britain

ATTENUATION IN THE EARTH AT LOW FREQUENCIES

BY G. MASTERS AND F. GILBERT
Institute of Geophysics and Planetary Physics, Scripps Institution of Oceanography, University of California at San Diego, La Jolla, California 92093, *U.S.A.*

(*Communicated by W. H. Munk, For.Mem.R.S. – Received* 26 *April* 1982)

CONTENTS

The introduction of global, digitally recording, seismic networks has provided the seismological community with a large quantity of high quality data. At low frequencies the IDA (International Deployment of Accelerometers) network provides the best available data and, in this report, over 500 IDA records have been carefully analysed giving nearly 4000 reliable measurements of centre frequency and apparent attenuation of fundamental spheroidal modes. The attenuation rate of a normal mode of free oscillation of the Earth is measured in terms of its Q or quality factor and mean Q values for the modes ${}_0S_8$–${}_0S_{46}$ are presented with standard deviations of 2–9 %. Mean centre frequencies have relative standard deviation of 5×10^{-5} to 5×10^{-4}. The distribution of the centre frequencies reveals a large-scale aspherical structure in velocity and density but the distribution of the apparent attenuation measurements does not reveal a corresponding structure.

A total of 26 new measurements of the mean Q of overtone modes with standard deviations of 5–30 % have also been obtained by using single-record and multiple-record techniques. Combining the new data with reliable Q measurements from the literature gives a total of 71 data with which we can infer the radial structure of attenuation inside the Earth.

This structure is not well constrained in detail and very simple models are capable of fitting the data. Experiments with synthetic data show that an improvement of an order of magnitude in both the number and quality of the measurements is required to make detailed inferences about the structure of attenuation.

The data do constrain the average shear Q^{-1} in the inner core to be 1/3500 (± 60 %) and the average shear Q^{-1} in the mantle to be 1/250 (± 4 %). These values are appropriate for frequencies less than 5 mHz. Comparison with published values at higher frequencies indicates there is a measurable frequency dependence of attenuation

between 3 and 30 mHz. Very little can be inferred about bulk dissipation in the Earth beyond that it must exist to satisfy the attenuation of the radial modes. Experiments show that the data can be satisfied if bulk attenuation is an average 1.3 %, or more, of the shear attenuation. Constraining bulk attenuation to be no greater than 2 % of the shear attenuation, and constraining the outer core to have no attenuation, forces bulk attenuation to be concentrated in the upper mantle.

1. Introduction

A knowledge of the distribution of density and elasticity in the Earth plays a central role in our inferences about chemical composition, phase changes, and the evolution of the structure of the Earth. In a similar way knowledge of the distribution of anelasticity provides additional constraints on our working hypotheses. Unfortunately, our knowledge of anelasticity is much poorer than our knowledge of elasticity and density. This is caused by the difficulty of isolating and accurately measuring attenuation effects in seismic records. In this paper we present an extensive set of observations of attenuation and discuss models of attenuation, and their resolvable features, compatible with the observations.

At low frequencies it is convenient to use the theory of free oscillations to describe observations. In this theory (Aki & Richards 1980; Lapwood & Usami 1981) a particular mode of oscillation is represented by

$$a_0(t) = A_0 \cos(\omega_0 t + \phi_0)\, \mathrm{e}^{-\alpha_0 t}. \tag{1}$$

The mode is characterized by initial amplitude, A_0, initial phase, ϕ_0, frequency, ω_0, and attenuation, α_0. It is useful to write

$$\alpha_0 = \omega_0 / 2Q_0, \tag{2}$$

where Q_0 is the 'quality' of the oscillation.

In the presence of noise one seeks to estimate the four parameters of each mode. Dahlen (1976, 1982) has shown that, for a least-squares estimator of the parameters of an isolated mode,

$$\mathrm{var}\,(\alpha_0) = \langle \alpha_0^2 \rangle = \mathrm{var}\,(\omega_0) = \langle \omega_0^2 \rangle, \tag{3}$$

i.e. that frequency and attenuation have the same variance. Let

$$\sigma_\alpha = \langle \alpha_0^2 \rangle^{\frac{1}{2}} / \alpha_0, \quad \sigma_\omega = \langle \omega_0^2 \rangle^{\frac{1}{2}} / \omega_0. \tag{4}$$

Then (2) and (3) show

$$\sigma_\alpha = 2Q_0 \sigma_\omega. \tag{5}$$

The relative standard deviation in attenuation is $2Q_0$ larger than the relative standard deviation in frequency. The frequency of a fundamental mode with a Q of about 200 can typically be measured to 0.05 %; the corresponding relative error in α is 20 %. Clearly, even in the absence of bias due to interference effects, accurate Q measurements are difficult to make and consequently our resolution of attenuation structure in the Earth is poor.

We shall use the notation $q = Q^{-1}$. Our observational data consist of pairs of ω_0, α_0, which we convert to q using (2). We shall restrict our attention to the radial distribution of attenuation and adopt the linear model

$$q_j = \int_0^a [q_\kappa(r)\, K_j(r) + q_\mu(r)\, M_j(r)]\, \mathrm{d}r \quad (j = 1, \ldots, J), \tag{6}$$

(Sailor & Dziewonski 1978; Backus & Gilbert 1967). Given a model of elasticity and density one can calculate $K_j(r)$ and $M_j(r)$ for the jth datum q_j, and (6) represents a linear inverse problem for $q_\kappa(r)$ and $q_\mu(r)$, the bulk and shear attenuation functions, respectively. The data are of insufficient quantity and quality to constrain any frequency dependence for $q_\kappa(r)$ and $q_\mu(r)$, so a frequency-independent model is assumed.

In solving (6) we take account of the errors in the data, q_j. If σ_q is the relative standard deviation in q we have from (2)–(4)

$$\sigma_q = \sigma_\alpha. \tag{7}$$

Thus the assigned standard deviation, ϵ_j, in the datum, q_j, is

$$\epsilon_j = \sigma_q q_j = \sigma_\alpha q_j. \tag{8}$$

Our data set will consist of $(q_j, \epsilon_j), j = 1, \ldots, J$.

At low frequencies the free oscillations occur in multiplets well enough separated in frequency to appear in the spectra as resonance peaks. Except for the radial modes, each multiplet consists of a number of singlets closely spaced in frequency. If the Earth were spherically symmetric the singlets in a multiplet would have a common, degenerate frequency and a common, degenerate attenuation. The actual frequency structure of the multiplet, termed splitting, is caused by rotation, ellipticity of figure and lateral heterogeneity of structure and gives rise to a beating pattern for each multiplet in the time domain. At very low frequencies or low angular orders the splitting can be resolved (Buland *et al.* 1978; Masters & Gilbert 1981) and the complex frequency, $\omega_0 + i\alpha_0$, can be measured for each well excited singlet. Unfortunately, for most multiplets at low frequencies the splitting cannot be resolved. Attenuation and finite record length make the singlet peaks overlap. Spatial filtering (e.g. stacking) requires a knowledge of the geographical shape of each singlet, which, in turn, requires a knowledge of the structure of lateral heterogeneity. Simple models of lateral heterogeneity are now becoming available (Masters *et al.* 1982) but are not presently well developed enough for stacking purposes.

Fortunately, multiplets often look like singlets and Dahlen (1979, 1981) has shown that, if the wavelength of the mode is short compared with the dominant wavelength of the lateral heterogeneity, a stationary-phase phenomenon gives rise to singlet cancellation resulting in a spectral line broadened by attenuation alone. This result is correct asymptotically in l, the total angular order of the multiplet. We have performed a search for singlet-like multiplets using 557 records from the IDA network. The IDA station codes and locations are given in Appendix B. We have primarily confined ourselves to the well excited fundamental modes but several isolated overtones have also been investigated. It is our experience that most spectral lines are not adequately modelled by single decaying cosinusoids and the apparent Q that is measured is strongly contaminated by interference effects from beating between singlets and from adjacent multiplets. This probably accounts for the large scatter of normal mode Q measurements in the literature (see for example Anderson & Hart 1978; Sailor & Dziewonski 1978; Geller & Stein 1979). It should be pointed out that no mode can be regarded as isolated in the spectrum. The reason for this is that the spectrum of a resonance peak falls off only at 6 dB/octave so that interference between adjacent fundamental modes is quite severe (Dahlen 1982; Silver & Jordan 1981). The presence of overtones between the fundamental modes exacerbates the problem. A simple way of improving the situation is to taper the records in the time domain. Application of a taper not only reduces spectral leakage associated with a finite record length but also modifies the spectrum of a resonance peak. For example, the use of a Hanning taper produces a modified spectrum that falls off at *ca.* 18 dB/octave, which means that all but the most closely spaced modes can be regarded as isolated. If tapering or some other method of modifying the spectrum is not used significant bias is introduced into the estimate of complex frequency.

To illustrate the effect of splitting on apparent attenuation we consider the reasonably well isolated fundamental mode, ${}_0S_{16}$, so as to minimize interference from adjacent multiplets. We

have used seven IDA records from the Sumbawa earthquake of 1977. This event is one of the largest recorded by the IDA network and the high signal levels allow long records to be used without significant deterioration in the results due to random noise sources. A complex frequency

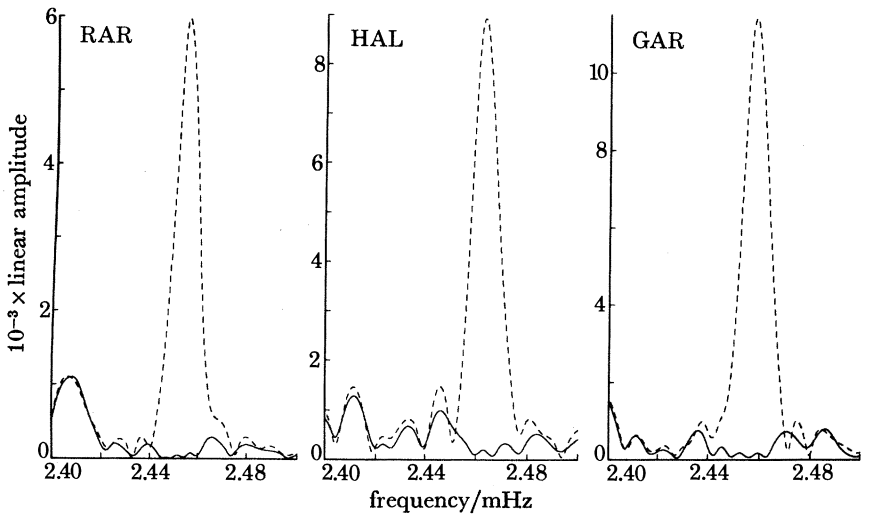

FIGURE 1. Three examples of successful demoding for the mode ${}_0S_{16}$ from records of the Sumbawa earthquake of 1977. The original spectrum is shown by the dashed line and the residual spectrum is shown by the solid line. The peaks are apparently singlet-like and interference effects may be sufficiently small to give a reliable attenuation estimate.

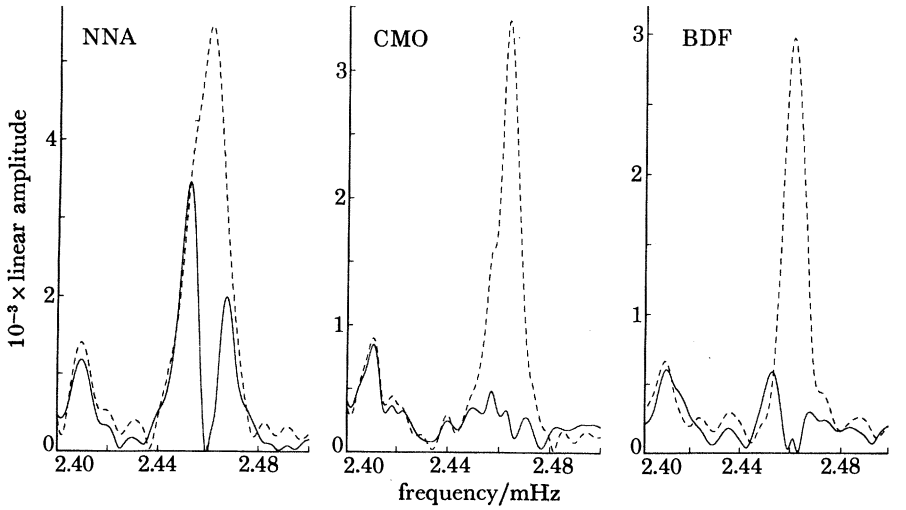

FIGURE 2. Three examples of unsuccessful demoding for the mode ${}_0S_{16}$ from records of the Sumbawa earthquake of 1977. The large residual spectrum shows that the peaks are not singlet-like and the measured attenuation rate is dominated by interference effects.

and amplitude measurement can be made by one of several methods (see next section) assuming that the line is singlet-like, and a residual spectrum computed by subtracting the measured mode from the record. The construction of a residual spectrum, a process we call demoding, is useful in determining how singlet-like the line really is. The measurement technique used in this example is described in Appendix A and in four out of the seven records the spectral line corresponding to

the multiplet ${}_0S_{16}$ is adequately modelled by a singlet (figure 1). In the other three cases this is not true (figure 2) and the residual spectrum is indicative of significant temporal beating (frequency splitting) between the singlets of ${}_0S_{16}$.

We have also found that beating effects lead to an apparent Q that varies as a function of record length and the results for the example given above are shown in table 1. For the three poorly demoded lines the Q and/or the apparent centre frequency varies strongly as the record length increases. The mean q value of the four stable measurements is about 1/290 and the analysis of many more records with demoding and variable record lengths to discriminate against split multiplets gives a value of 1/287 ($\pm 2\%$). A large data set is required to gain this precision as a multiplet is only singlet-like in 20–30 % of cases. Furthermore, many determinations of complex frequency are required, demanding a cheap and efficient estimation technique.

TABLE 1. VARIATION OF THE COMPLEX FREQUENCY OF ${}_0S_{16}$ WITH RECORD LENGTH

station	record length h	frequency mHz	Q
NNA	30	2.4663	280
	60	2.4604	740
	90	2.4588	505
CMO	30	2.4625	221
	60	2.4634	210
	90	2.4639	226
BDF	30	2.4631	667
	60	2.4610	575
	90	2.4605	448
RAR	30	2.4550	256
	60	2.4548	274
	90	2.4549	268
SUR	30	2.4603	338
	60	2.4603	320
	90	2.4600	307
HAL	30	2.4634	288
	60	2.4632	284
	90	2.4631	274
GAR	30	2.4580	276
	60	2.4584	273
	90	2.4583	264

A comparison of techniques is given in the next section. This is followed by a description of the data analysis where we have mainly confined ourselves to measurements from single records. We have avoided measuring Q from multiplet stacks as it is known that this leads to biased estimates (Dahlen 1979). Stacking for singlets is possible and desirable for modes of high Q and low angular order (Riedesel *et al.* 1980; Chao & Gilbert 1980; Buland *et al.* 1978) and we present some new results using this method though a detailed description will be given elsewhere.

2. ESTIMATION OF COMPLEX FREQUENCIES

The traditional method for measuring α_0 in (1) is the time lapse method. Smith (1972) reviews the early observations, most of which were obtained by this method. For good s.n.r. (signal-to-noise ratio) it works well, and, for example, was the method used by Dratler *et al.* (1971) to discover high-Q overtone modes. However, it suffers from some adverse characteristics. It can be used

only on single modes and single records, it has poor variance characteristics for α_0 for a given s.n.r. (Emmerman & Dahlen 1979) leading to imprecise estimates and it is relatively costly. The method also does not easily lend itself to the application of tapers, which are essential to the estimation of Q.

Recently several new methods have become available. A method closely related to the time lapse method is given by Geller & Stein (1979). A narrow bandpass filter is used to isolate the mode of interest and the Hilbert transform is used to construct the envelope of the decay of the mode in the time domain. The method is limited to single mode determinations and is relatively costly. It also appears that beating, which is obvious in the frequency domain as spectral splitting, is not easily diagnosed by inspection of the decay envelope in the time domain. For example the decay envelope of the severely split multiplet ${}_0S_{16}$ at NNA (figure 2) looks like the decay envelope of a singlet (Geller & Stein 1979) leading to a spurious Q value.

Buland & Gilbert (1978) suggested the moment ratio technique for estimating the centre frequency and the minimum width technique for measuring Q. The minimum width method involves multiplying the record by a trial growing exponential, $e^{\alpha_T t}$. The estimator α_T is varied until a value that best cancels the effect of attenuation is found, i.e. when the width of the resulting spectral peak is minimized. No formal error analysis exists for this method, but the implied weighting of the latter part of the record where the s.n.r. is smallest suggests that α_T will be an imprecise estimator. Again, the method can only be applied to a single mode and is costly to implement. By contrast, the moment ratio method of estimating the centre frequency is very stable even when a mode shows signs of splitting. Bolt & Brillinger (1979) have described a complex demodulation technique in which they use a least squares estimator to retrieve the modal properties from the complex demodulator. Hansen (1982*a*) has also discussed the method in some detail and, in a later paper (Hansen 1982*b*), gives an application to 24 long-period recordings.

Two algorithms have been used in this work. The autoregressive (a.r.) method of Chao & Gilbert (1980) has proved to be fast and reliable and can be used for simultaneous multi-mode estimation. An error analysis also exists for this method allowing error estimates to be assigned to the measurements. Surprisingly, straightforward nonlinear least squares (l.s.) fitting of resonance peaks to data has apparently not been used and we describe one algorithm in detail in Appendix A. It turns out to be well known in estimation theory how to remove the linear part of an l.s. problem. In our case we decouple the estimation of complex amplitude and complex frequency. This makes the method stable and, because the matrix elements required can be computed analytically for any reasonable taper, the procedure is extremely fast. The algorithm can perform multi-mode estimation and the use of various tapers can be easily accommodated. The l.s. method allows Q measurements to be made faster than the computation of an f.F.t. and it is a little more efficient than the a.r. method. A comparison of the two techniques is given in the next section. Dahlen (1982) has given a detailed error analysis for l.s. methods explicitly incorporating the Hanning or Blackman–Harris minimum four-term tapers.

As we have stressed, tapering is essential to isolate modes in the spectrum but results in a degradation of s.n.r. and a broadening of the peak near the centre frequency. Harris (1978) gives a thorough review of the many tapers available and we have chosen the Hanning taper because the loss of s.n.r. is not so great as for the Blackman–Harris taper and the peak can be well characterized by fitting over a smaller frequency band. We have found that a mode is adequately characterized by sampling the spectrum at three–five points in a frequency band $3\alpha_0$

wide about the centre frequency. Intuitively one might think that a partial taper (e.g. a Cooley–Tukey 25 % cosine taper) might be useful. Such tapers do not weight down the initial part of the record as much as, say, the Hanning taper so that the loss of s.n.r. is not as great. Conversely they do not suppress spectral leakage very well. Harris (1978) shows that the spectral window of the Cooley–Tukey taper has a first side lobe only 14 dB down as compared with 13 dB down for the boxcar taper and 32 dB down for the Hanning taper. This high side-lobe level is undesirable in the applications discussed here.

Measurements of Q made without tapering should be viewed with the greatest suspicion and even the centre frequencies can be significantly biased at the accuracy levels possible with modern digital data (Dahlen 1982; Xu & Knopoff 1980). Almost all previous measurements of Q for free oscillations have been made without tapering.

If a nearby mode interferes with a measurement or if a multiplet is partially resolvably split we have usually chosen to discard the observation. Multi-mode estimates are possible but great care must be taken to assess the uniqueness of the results as trade-offs between the complex amplitudes and frequencies of individual lines are extremely common. If two closely spaced lines have very different attenuation rates then the Earth can be used as an attenuation filter by discarding the leading part of the record. If the signal level is sufficiently high, the low-Q line can be effectively removed from the spectrum by this method. The properties of the high-Q line can then be inferred with a single mode estimate. The properties of the low-Q line can be recovered by subtracting the high-Q line from the record or by using the inferred properties of the high-Q line as additional data in a multi-mode estimate. The latter procedure is preferable as subtraction of the high-Q line requires extrapolating its estimated complex amplitude back to the start time of the record and any errors in the estimate are exponentially amplified. If two closely spaced lines have similar attenuation rates, as for resolvably split multiplets, then a multimode estimate must be made. The uniqueness of the results can be investigated by making perturbations in the inferred complex frequencies, re-solving for the complex amplitudes, and computing the residual power in the demoded spectrum. In this way a family of solutions with acceptably small residual power can be constructed.

An illustration of the technique is given in figures 3 and 4. A spectrum of a recording made at the IDA station SUR of an event in Tonga shows that the mode ${}_{13}S_2$ is clearly split. If this mode is modelled as two singlets, the optimum fit to the data is given with frequencies of 4.8388 and 4.8448 mHz and both lines have Q of about 1050. The result of demoding the spectrum with these parameters is shown in figure 3. The complex frequencies are now perturbed, new complex amplitudes determined and a contour plot of the region of acceptable solutions constructed. This is shown in figure 4. The external contour corresponds to an average residual power level, which is roughly at the ambient noise level. Clearly the region of acceptable solutions based on the average residual power is rather large. Some of the solutions in this region show unacceptable structure in the demoded spectrum and a better measure of acceptability is probably the peak residual power rather than the average residual power. The shaded region encompasses all solutions with average residual power less than $\frac{1}{10}$ of the ambient noise level. The uncertainty in the attenuation estimates is still about 20 %. An isolated mode with this signal level would have an error in q of about 10 % and the additional uncertainty in the multi-mode estimate is due to the large trade-offs between the properties of the lines.

Unless signal levels are very high, multi-mode estimates from single records can be subject to large uncertainties. If a frequency band encompasses a known number of singlets it is possible

PHILOSOPHICAL TRANSACTIONS OF THE ROYAL SOCIETY A MATHEMATICAL, PHYSICAL & ENGINEERING SCIENCES

simultaneously to estimate the properties of all the singlets by using data from many recordings. Chao & Gilbert (1980) have used the a.r. technique to do this and the l.s. method can be extended in an obvious way to have this capability. The speed and flexibility of the l.s. and a.r. algorithms make them very attractive and will, we hope, ensure a decline in the use of the more traditional estimation methods, such as the time lapse method, in the future.

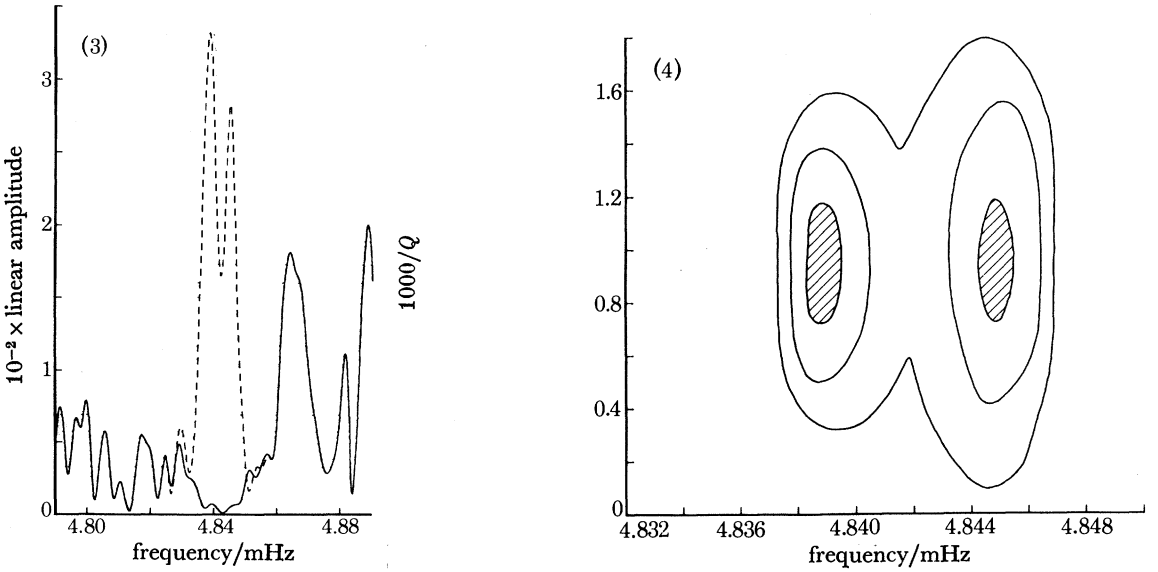

FIGURE 3. An example of a multi-mode estimate from records of an event in Tonga at the IDA station SUR. The two peaks (dashed line) are singlets of the mode $_{13}S_2$, their frequencies are 4.8388 and 4.8448 mHz and their Q values are both about 1050. This mode has a total of five singlets so interference effects cannot be ruled out. The Q value has been confirmed from other records. The solid line represents the demoded spectrum.

FIGURE 4. The region of acceptable complex frequency measurement for the example of figure 3 is shown by the external contour. The internal contours delineate the regions of acceptable solutions with residual power levels of 0.5 (outer) and 0.1 (inner) respectively of the ambient noise power level.

3. DATA ANALYSIS

The 557 IDA records used in this study are recordings from the events listed in table 2. For all but the largest events a maximum data length of 40 h was chosen. Each record was visually examined for instrumental nonlinearity and noise glitches (i.e. places where noise has invalidated the record). On most records the first passage of the Rayleigh wave saturates the instrument and the first 2 h of recording are lost. In such cases the data window is simply shifted forward. Short duration glitches have been linearly interpolated while longer gaps due to data loss or large aftershocks are flagged. The resulting panel structure of the data is incorporated into the frequency estimation techniques. The tidal signal is then removed by a process of least squares fitting. Events with large aftershocks or multiple events have been discarded; Q measurements from such records will obviously be corrupted. For a few larger events, up to 250 h of data have been prepared. These records are the main data base for looking at apparent singlets of modes of high Q and low angular order and very low frequency modes.

Dahlen (1982) has shown that the optimum record length for complex frequency estimation employing an l.s. technique with the Hanning window is about 1.1 Q cycles though it is possible to use 0.75–1.75 Q cycles with little loss of accuracy. The same is also roughly true of the a.r.

method (Chao & Gilbert 1980). With the 40 h records used in this study we have been able to analyse the fundamental modes from ${}_0S_8$ to ${}_0S_{46}$. Above ${}_0S_{46}$ it is difficult to find isolated singlet-like peaks as the mode spectrum becomes too dense at these frequencies. Below ${}_0S_8$ long records must be used to determine Q and, in addition, the asymptotic theory breaks down at low angular orders making singlet stacking essential for reliable attenuation measurements.

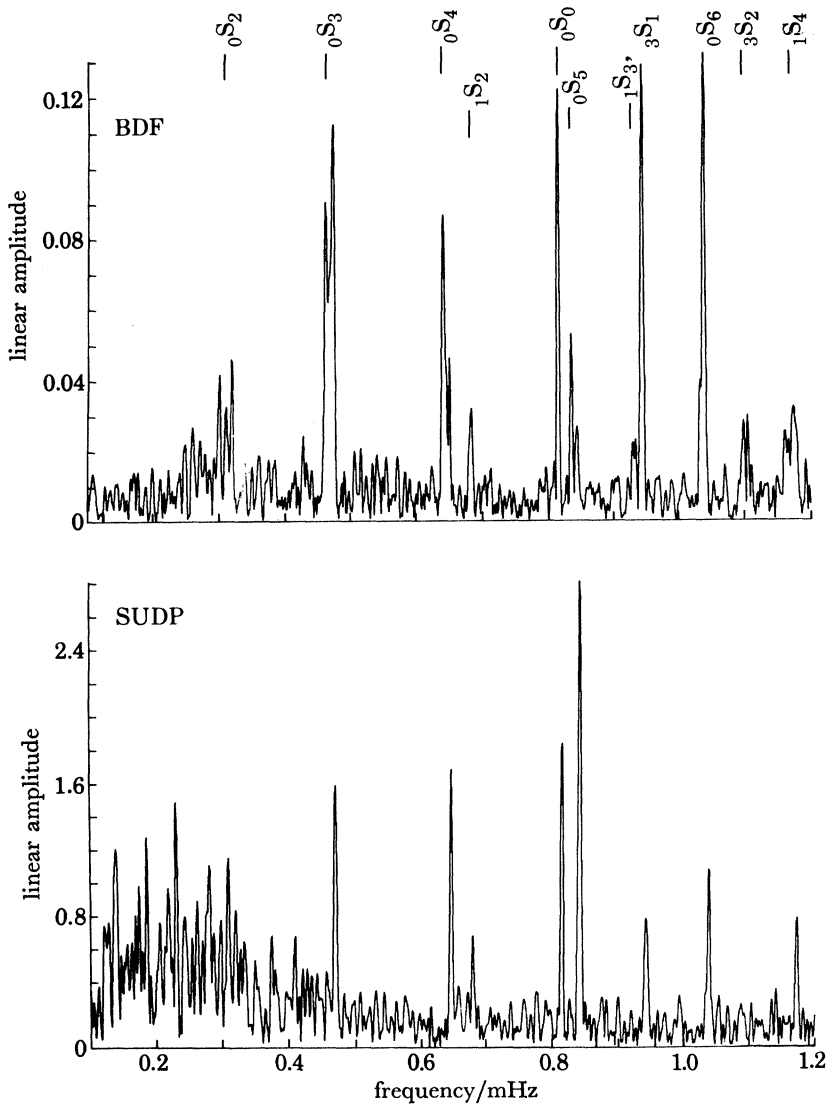

FIGURE 5. Two spectra of 120 h records from the Sumbawa earthquake of 1977. In the upper panel the effects of rotation and ellipticity cause obvious splitting of ${}_0S_2$–${}_0S_6$ at the IDA station at Brasilia (BDF; 1971, day 231 at 6 h 14 min 40 s). In the lower panel, the spectrum of the UCLA South Pole record (SUDP; 1977, day 231 at 6 h 10 min 10 s) shows no obvious splitting for ${}_0S_3$–${}_0S_5$. The mode ${}_0S_2$ is below the noise level and ${}_0S_6$ shows some signs of splitting.

To perform stacking, the singlet shape must be known though it appears that simple geographical spherical harmonics adequately model the shape for $l \lesssim 5$. If this is true then records from the South Pole will show only the ${}_nS_l^0$ line. Figure 5 shows such a record compared with the

TABLE 2. LOCATIONS AND ORIGIN TIMES OF EARTHQUAKES RECORDED BY THE IDA ARRAY

year	day	h	min	s	lat.	long.	depth/km	number of records
1975	189	12	4	42.4	21.49° N	94.70° E	157	1
1975	201	14	37	39.9	6.59° S	155.04° E	49	1
1975	274	3	29	58.9	4.88° S	102.20° E	33	1
1975	279	22	24	16.2	12.52° S	166.50° E	54	1
1975	284	14	35	15.0	24.89° S	175.12° W	9	1
1975	304	8	28	2.6	12.54° N	125.99° E	50	2
1975	333	14	47	40.4	19.33° N	155.02° W	5	2
1976	1	1	29	39.6	28.61° S	177.64° W	59	2
1976	14	15	56	34.9	29.21° S	177.89° W	69	1
1976	21	10	5	24.1	44.92° N	149.12° E	41	3
1976	35	9	1	43.4	15.32° N	89.10° W	5	3
1976	64	2	50	0.5	14.74° N	167.10° E	90	2
1976	84	4	46	4.4	29.89° S	177.87° W	33	3
1976	99	2	40	27.0	40.31° N	63.77° E	10	2
1976	126	4	52	51.0	29.93° S	177.84° W	35	2
1976	144	6	1	14.6	4.94° S	153.69° E	103	2
1976	155	16	44	38.8	5.20° S	153.44° E	88	2
1976	172	20	53	13.4	3.40° N	96.32° E	33	3
1976	177	19	18	56.9	4.60° S	140.09° E	33	2
1976	209	19	42	54.6	39.57° N	117.98° E	23	1
1976	215	10	55	25.7	20.61° S	169.27° E	52	1
1976	303	2	51	7.6	4.52° S	140.00° E	33	2
1976	312	17	9	6.1	8.48° N	126.37° E	60	2
1976	335	0	40	57.8	20.52° S	68.92° W	82	3
1977	17	21	27	12.6	24.85° S	68.67° W	26	2
1977	63	19	21	54.1	45.77° N	26.76° E	94	5
1977	77	21	43	52.4	16.77° N	122.33° E	37	5
1977	92	7	15	22.7	16.70° S	172.10° W	33	6
1977	173	12	8	33.4	22.88° S	175.90° W	65	7
1977	210	11	15	45.3	8.03° S	155.54° E	33	7
1977	223	1	42	47.5	17.56° S	174.37° W	57	5
1977	231	6	8	55.2	11.09° S	118.46° E	33	7
1977	283	11	53	53.6	25.86° S	175.41° W	24	8
1977	290	17	26	40.4	27.91° S	173.08° E	33	8
1977	327	9	26	24.7	31.03° S	67.77° W	12	6
1978	14	3	24	39.0	34.81° N	139.26° E	14	1
1978	40	21	35	12.7	30.68° S	177.36° W	33	1
1978	66	2	48	47.6	32.00° N	137.61° E	439	9
1978	100	20	52	18.9	11.36° S	116.69° E	33	7
1978	133	7	8	46.2	14.52° S	167.32° E	160	10
1978	163	8	14	26.4	38.19° N	142.03° E	44	7
1978	165	12	32	33.9	8.25° N	122.40° E	24	7
1978	168	15	11	33.5	17.10° S	172.26° W	33	7
1978	204	14	42	36.9	22.28° N	121.51° E	17	8
1978	215	18	11	17.1	26.51° S	70.54° W	58	1
1978	259	15	35	56.6	33.39° N	57.43° E	33	9
1978	266	16	32	11.1	13.92° S	167.21° E	201	9
1978	309	22	2	7.1	11.13° S	162.14° E	33	9
1978	333	19	52	47.6	16.01° N	96.59° W	18	9
1978	340	14	2	1.0	44.59° N	146.58° E	91	10
1978	346	11	44	16.0	7.33° N	123.49° E	33	10
1978	357	11	23	12.0	23.25° N	122.08° E	33	9
1979	47	10	8	53.4	16.39° S	72.66° W	53	8
1979	59	21	27	6.1	60.64° N	141.59° W	15	9
1979	73	11	7	16.3	17.81° N	101.28° W	49	10
1979	100	1	42	22.0	2.96° N	126.93° E	37	7
1979	121	13	3	37.1	21.24° S	169.80° E	79	11
1979	140	8	14	0.1	56.65° N	156.73° W	71	5

PHILOSOPHICAL TRANSACTIONS OF THE ROYAL SOCIETY A MATHEMATICAL, PHYSICAL & ENGINEERING SCIENCES

TABLE 2. (*cont.*)

year	day	h min s	lat.	long.	depth/km	number of records
1979	141	22 22 23.6	15.25° S	70.09° W	208	9
1979	173	6 30 54.3	17.00° N	94.61° W	107	10
1979	176	5 29 5.6	4.98° S	145.58° E	189	8
1979	205	19 31 19.8	11.15° S	107.71° E	31	11
1979	217	0 53 45.9	22.72° S	177.49° W	181	6
1979	237	8 44 4.0	10.73° N	41.69° W	10	8
1979	238	14 31 22.1	19.07° N	122.10° E	15	9
1979	255	5 17 51.4	1.68° S	136.04° E	5	7
1979	272	18 37 12.5	1.19° N	94.25° E	27	10
1979	285	10 25 22.3	46.68° S	165.71° E	33	9
1979	296	9 51 6.7	10.62° S	161.28° E	22	8
1979	320	15 21 25.7	16.76° S	179.98° E	33	8
1979	327	23 40 29.8	4.81° N	76.22° W	108	9
1979	331	17 10 32.9	33.96° N	59.73° E	10	8
1979	346	7 59 3.3	1.60° N	79.36° W	24	10
1980	38	10 49 16.0	54.16° S	158.89° E	10	4
1980	54	5 51 3.2	45.53° N	146.75° E	44	10
1980	58	21 17 20.2	6.02° S	150.19° E	53	7
1980	68	22 12 10.3	22.68° S	171.36° E	38	9
1980	84	3 59 51.3	52.97° N	167.67° W	33	7
1980	104	18 4 31.9	23.47° S	177.30° W	79	8
1980	177	23 18 20.4	5.23° S	151.69° E	49	9
1980	190	23 19 19.8	12.41° S	166.38° E	33	9
1980	198	19 56 46.7	4.46° S	143.52° E	84	10
1980	199	19 42 23.2	12.53° S	165.92° E	33	9
1980	222	5 45 9.5	15.89° N	88.52° W	22	8
1980	284	12 25 23.5	36.20° N	1.35° E	10	9
1980	313	10 27 34.0	41.12° N	124.25° W	19	11
1980	316	10 36 58.2	51.42° S	28.80° E	10	8
1980	328	18 34 53.8	40.91° N	15.36° E	10	9
1980	352	16 21 58.8	49.48° N	129.50° W	10	10
1980	366	10 32 11.1	46.06° N	151.45° E	33	6

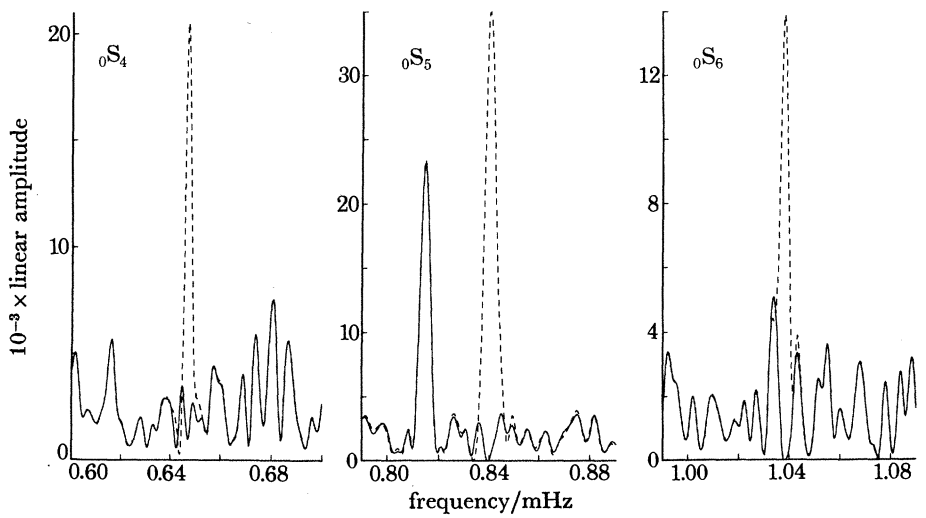

FIGURE 6. Demoding of $_0S_4$–$_0S_6$ at the South Pole from records of the Sumbawa earthquake of 1977. The residual spectrum of $_0S_6$ is indicative of splitting and gives rise to a spuriously high Q value of 720. The apparent Q values of $_0S_4$ and $_0S_5$ are 390 and 300 respectively and their residual spectra show no features above the ambient noise level.

PHILOSOPHICAL TRANSACTIONS OF THE ROYAL SOCIETY A MATHEMATICAL, PHYSICAL & ENGINEERING SCIENCES

BDF recording of the same event. The mode ${}_0S_6$ is obviously split on this record while ${}_0S_4$ and ${}_0S_5$ appear to be singlet-like (figure 6). The Q value for ${}_0S_5$ is suspiciously low and singlets other than ${}_0S_5^0$ may be present. This work is still in progress and we have only a few accurate Q measurements for the modes ${}_0S_2$–${}_0S_6$. It is our experience that attempts to measure singlets from individual records do not give reliable answers as the s.n.r. is too low and interference effects are generally important. These problems are reflected in the large scatter of Q measurements for these modes (see also Stein & Nunn 1981).

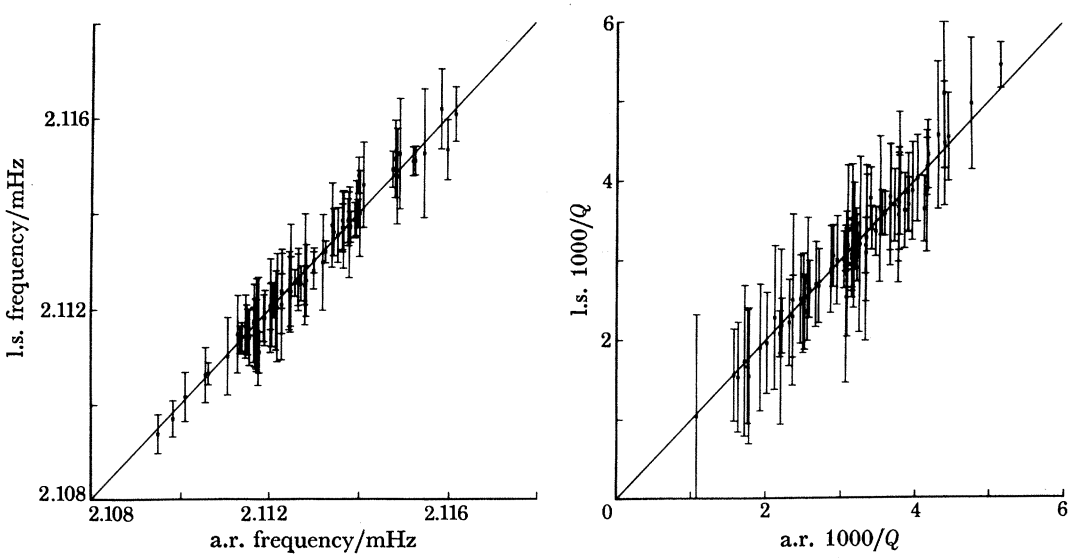

FIGURE 7. A comparison of the apparent centre frequency and apparent attenuation rate from the a.r. and l.s. techniques for the mode ${}_0S_{13}$. In practically all cases the two techniques give the same result within one standard deviation. There is clearly a measurable variation in both quantities though the large variation in apparent attenuation rate cannot be easily explained.

The first experiment we performed on the large data set was the comparison of the a.r. method and the l.s. algorithm presented in Appendix A. A measurement was considered acceptable if the synthetic peak derived from the procedures fitted the data at five points between the half power points with a root mean square (r.m.s.) residual of better than 5%. The demoded spectrum was then visually examined and modes obviously contaminated by interference effects discarded. The results for the mode ${}_0S_{13}$ are shown in figure 7. For well isolated, high signal peaks the methods give almost identical results for both apparent centre frequency and q. There is no detectable bias in the observations as the means of centre frequency and q are the same within the errors for both techniques. It is inconceivable that the large observed variation in apparent q is due to lateral structure in attenuation alone though the peaks appear very singlet-like to both methods. This problem is discussed in detail below. Chao (1981) has compared the methods for the radial modes ${}_2S_0$–${}_6S_0$ and the results are again the same within the observational errors. For the purposes of this paper there is very little to choose between the techniques so, because the a.r. method is marginally less efficient, we have used the l.s. method in the following.

The results of an analysis of the fundamental modes ${}_0S_8$–${}_0S_{46}$ are summarized in table 3*a*. Each peak was assigned an s.n.r., with the demoded spectrum as a guide, and an error in the complex frequency was computed by using the results of Dahlen (1982). We have tried assigning signal levels automatically by computing the residual power in the demoded spectrum (Riedesel *et al.*

1980). However, synthetic experiments show that some noise is also removed in the fitting procedure, leading to erroneously high s.n.r. estimates. The ambient noise level has been assessed from the apparent noise level in a 0.2 mHz band surrounding the mode. The assigned errors can only be regarded as qualitatively correct as they are based on a subjective assessment of signal level and on the assumption that the mode is an isolated singlet. If the record length used in the analysis is varied then acceptable measurements of complex frequency vary by less than the assigned errors so we feel we have probably been conservative in the assessment of s.n.r. The record length used at high angular orders is somewhat greater than optimum (*ca.* 1.5 Q cycles) but it was found that, if a shorter record was used, truncation effects made visual assessment of contamination by adjacent modes almost impossible.

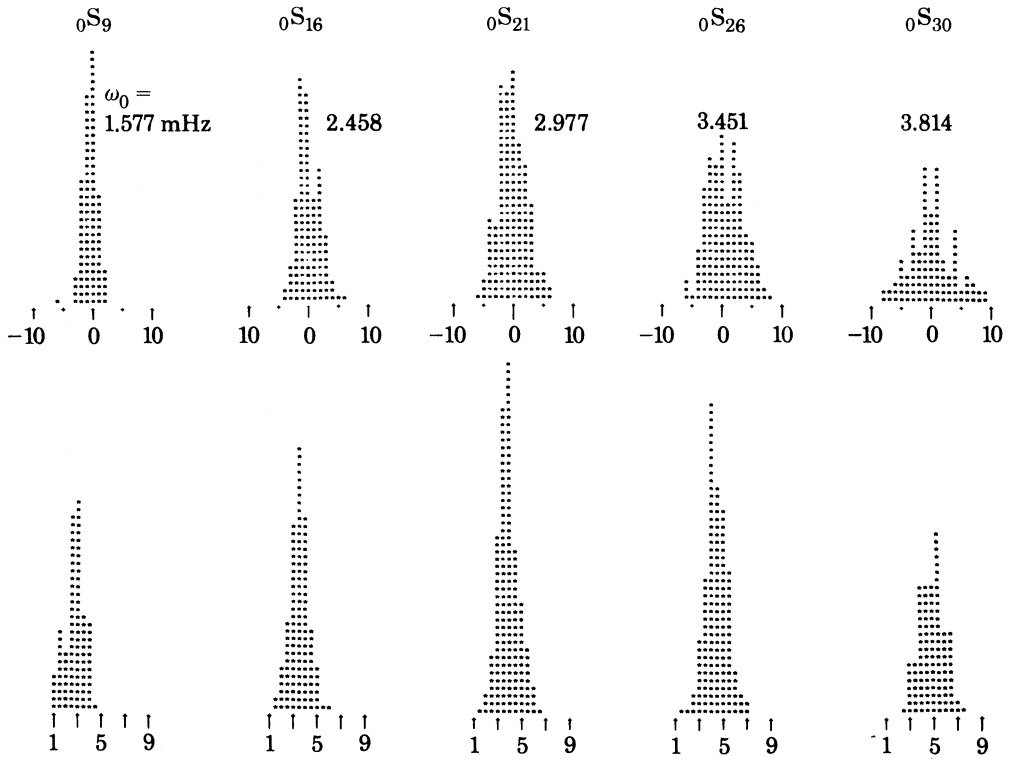

FIGURE 8. Histograms of apparent centre frequency and $1000/Q$ of singlet-like fundamental modes. The upper histograms are of centre frequency; each symbol represents a measurement and the horizontal scale shows the deviation, in microhertz, from the reference frequency. The lower histograms are of $1000/Q$ and the coarseness of the horizontal scale reflects the large scatter in these measurements.

Figure 8 shows histograms of centre frequency and $1000/Q$ for five of the fundamental modes. The variation in centre frequency is due dominantly to the effects of lateral heterogeneity. If the wavelength of the dominant lateral heterogeneity is much longer than the wavelength of the mode then the asymptotic theory developed by Jordan (1978) and Dahlen (1979, 1981) shows that the peak location is a function only of the pole position of the great circle joining source and receiver. This is verified in figure 9 and Masters *et al.* (1982) have shown that simple degree-two models of lateral heterogeneity can account for between 60 % and 80 % of the variance in the frequency measurements. If the effect of the dominant degree-two inhomogeneity is removed from the frequency measurements the histograms are modified as shown in figure 10. The corrected histo-

TABLE 3. OBSERVATIONS OF MEAN MODE FREQUENCIES AND ATTENUATIONS

mode	frequency mHz	s.d. (%)	$1000/Q$	s.d. (%)	number of observations
		(*a*) Fundamental spheroidal modes			
${}_0S_8$	1.4124	0.011	2.805	7.0	66
${}_0S_9$	1.5767	0.006	2.945	4.0	104
${}_0S_{10}$	1.7238	0.006	3.044	5.0	100
${}_0S_{11}$	1.8626	0.027	4.155	9.0	35
${}_0S_{12}$	1.9909	0.008	3.219	4.0	93
${}_0S_{13}$	2.1130	0.005	3.114	3.0	158
${}_0S_{14}$	2.2309	0.007	3.401	3.0	105
${}_0S_{15}$	2.3461	0.006	3.146	3.0	124
${}_0S_{16}$	2.4582	0.006	3.484	2.0	125
${}_0S_{17}$	2.5674	0.006	3.712	3.0	113
${}_0S_{18}$	2.6734	0.007	3.978	3.0	127
${}_0S_{19}$	2.7758	0.014	4.329	3.0	129
${}_0S_{20}$	2.8766	0.007	3.935	4.0	110
${}_0S_{21}$	2.9761	0.005	3.805	2.0	175
${}_0S_{22}$	3.0739	0.005	3.947	3.0	158
${}_0S_{23}$	3.1704	0.005	4.038	2.0	217
${}_0S_{24}$	3.2651	0.006	4.052	4.0	118
${}_0S_{25}$	3.3587	0.006	4.437	4.0	131
${}_0S_{26}$	3.4515	0.006	4.397	3.0	161
${}_0S_{27}$	3.5431	0.006	4.570	3.0	160
${}_0S_{28}$	3.6343	0.007	4.720	3.0	158
${}_0S_{29}$	3.7243	0.005	4.696	3.0	193
${}_0S_{30}$	3.8144	0.008	4.825	4.0	115
${}_0S_{31}$	3.9049	0.010	5.071	4.0	111
${}_0S_{32}$	3.9942	0.013	5.015	4.0	91
${}_0S_{33}$	4.0832	0.007	5.573	3.0	146
${}_0S_{34}$	4.1713	0.010	5.487	4.0	87
${}_0S_{35}$	4.2616	0.012	5.719	4.0	59
${}_0S_{36}$	4.3511	0.009	5.595	3.0	92
${}_0S_{37}$	4.4407	0.009	5.583	3.0	79
${}_0S_{38}$	4.5301	0.009	5.679	2.0	87
${}_0S_{39}$	4.6192	0.022	6.122	5.0	41
${}_0S_{40}$	4.7080	0.021	6.176	5.0	41
${}_0S_{41}$	4.7982	0.013	6.156	4.0	40
${}_0S_{42}$	4.8886	0.031	6.096	8.0	13
${}_0S_{43}$	4.9772	0.020	6.604	6.0	24
${}_0S_{44}$	5.0692	0.050	6.693	7.0	16
${}_0S_{45}$	5.1557	0.050	6.802	7.0	17
${}_0S_{46}$	5.2490	0.050	6.805	7.0	15
		(*b*) Overtone spheroidal modes			
${}_2S_6$	1.6808	0.035	4.250	18.0	16
${}_2S_8$	2.0505	0.020	4.403	7.0	48
${}_2S_{10}$	2.4031	0.030	5.183	10.0	35
${}_2S_{12}$	2.7384	0.050	5.364	15.0	9
${}_5S_3$	2.1681	0.030	2.946	17.0	15
${}_5S_4$	2.3793	0.025	2.189	22.0	25
${}_5S_5$	2.7028	0.025	1.956	24.0	21
${}_5S_6$	3.0106	0.015	1.998	15.0	23
${}_5S_7$	3.2916	0.040	2.088	29.0	9
		(*c*) Radial modes and miscellaneous measurements			
					comments
${}_0S_0$	0.814664	0.0004	0.175	5.0	†
${}_1S_0$	1.63151	0.003	0.541	12.0	†
${}_2S_0$	2.5079	0.010	0.555	25.0	Payson

PHILOSOPHICAL TRANSACTIONS OF THE ROYAL SOCIETY A MATHEMATICAL, PHYSICAL & ENGINEERING SCIENCES

TABLE 3. (*cont.*)

mode	frequency / mHz	s.d. (%)	1000/Q	(%)	number of observations
	(*c*) Radial modes and miscellaneous measurements				comments
${}_3S_0$	3.2723	0.004	0.709	10.0	Payson
${}_4S_0$	4.1062	0.002	0.823	5.0	Payson
${}_5S_0$	4.8891	0.004	0.800	10.0	Payson
${}_6S_0$	5.7423	0.006	0.870	17.0	Payson
${}_6S_2$	2.4398	0.010	0.345	70.0	‡
${}_7S_3$	3.1139	0.010	0.357	60.0	‡
${}_0S_3$	0.4682	0.046	3.333	28.0	S. Pole
${}_0S_4$	0.6471	0.029	2.557	23.0	S. Pole
${}_0S_5$	0.8403	0.012	3.268	7.0	S. Pole
${}_0S_7$	1.2327	0.010	2.898	7.0	S. Pole
${}_1S_4$	1.1735	0.039	3.367	23.0	S. Pole
${}_2S_3$	1.2456	0.020	1.852	18.0	S. Pole
${}_8S_1$	2.8710	0.008	1.399	11.0	Payson
${}_{13}S_1$	4.4889	0.008	1.515	11.0	Payson
${}_3S_1$	various singlets		1.111	11.0	stacking
${}_3S_2$	various singlets		2.273	25.0	stacking
${}_5S_2$	various singlets		3.175	10.0	stacking
${}_{10}S_2$	various singlets		0.926	10.0	stacking
${}_{13}S_2$	various singlets		0.976	10.0	stacking
${}_1S_3$	various singlets		2.941	15.0	stacking

† Riedesel *et al.* (1980). ‡ Masters & Gilbert (1981).

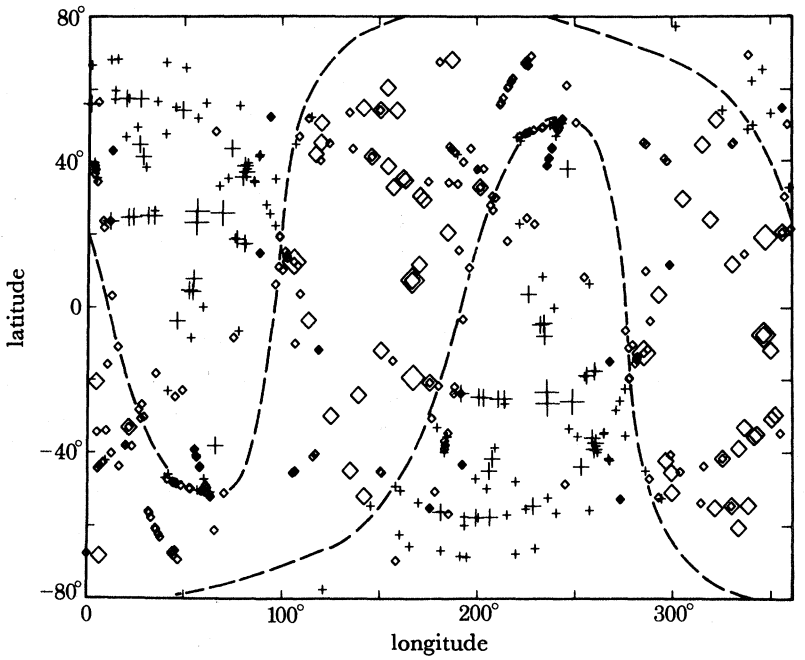

FIGURE 9. The effect of aspherical structure on centre frequency can be seen by plotting the shift in frequency as a function of the pole position of the great circle joining source and receiver. Each symbol is plotted at a pole position: a + corresponds to a positive frequency shift (relative to the frequencies given in table 3*a*) and a ◇ corresponds to a negative frequency shift. The size of the symbol is indicative of the magnitude of the shift: the smallest symbols correspond to a 0–0.1% shift and the largest to a 0.3–0.4% shift. A degree-two spherical harmonic pattern accounts for most of the structure in the observations; the nodal lines of this pattern are shown by the dashed lines. This example is a combination of measurements for the modes ${}_0S_{21}$–${}_0S_{23}$.

grams are much more Gaussian in nature, and bias in the mean frequency due to inadequate sampling of the sphere is reduced. We have tried to incorporate these effects in the means and error estimates given in table 3.

Asymptotic theory gives an acceptable description of the variation in apparent centre frequencies and, according to Dahlen (1981), the variation in apparent attenuation due to lateral

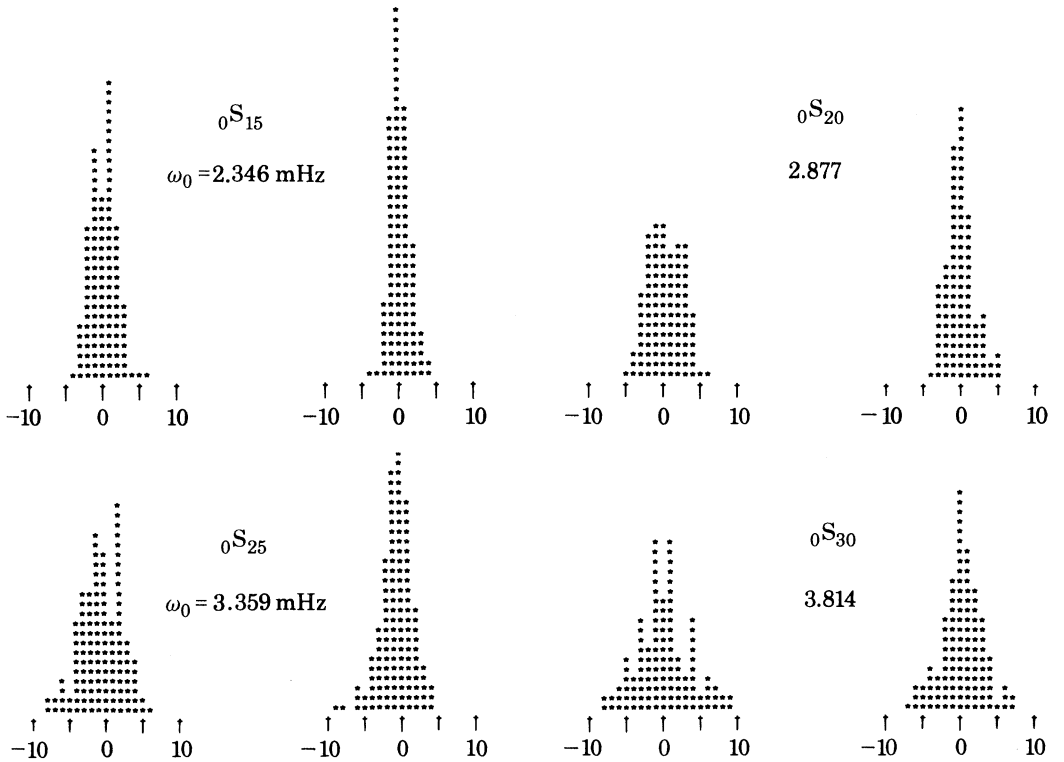

FIGURE 10. Examples of histograms of apparent centre frequency of modes $_0S_l$ before (right) and after (left) removing the dominant degree-two signal from aspherical structure. This signal accounts for 50–80 % of the variance in the frequency histograms between $_0S_{16}$ and $_0S_{38}$. The corrected histograms are much more Gaussian in nature and their means can differ from the means of the raw data by up to 0.5 μHz.

heterogeneity should be similarly described. Figure 11 shows shifts in $1000/Q$ (relative to the means given in table 3) as a function of pole position. Intuitively one would expect that an anomalously high frequency should correlate with an anomalously low attenuation rate so that figure 11 should look like figure 9 but with reversed sign. The expected correlation is clearly absent and no simple pattern appears at all. Another way of looking at the correlation is shown in figure 12 where $1000/Q$ is plotted against frequency for the two modes $_0S_{16}$ and $_0S_{23}$ (for clarity, only measurements of $1000/Q$ with precision better than 10 % are shown). Again there appears to be no significant trend in the data.

The reason for the lack of correlation is not clear. First-order perturbation theory, upon which Dahlen's analysis is based, is accurate to first order in the eigenfrequencies and to zero order in the eigenfunctions. To this order the integrated complex amplitude of a mode is insensitive to lateral heterogeneity (Jordan 1978). The predicted insensitivity is not observed in practice (Riedesel *et al.* 1980) and complicates source retrieval for long period data. The variability of complex amplitude suggests that perturbations to the eigenfunctions may be important and may give rise

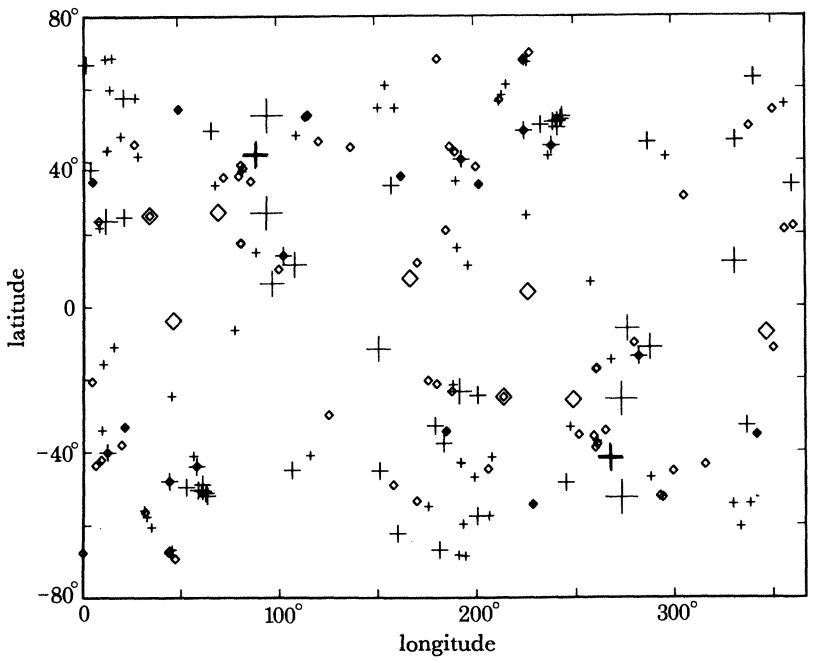

FIGURE 11. Shifts in $1000/Q$ as a function of pole position (see caption to figure 9). The smallest symbols correspond to shifts of 0–20% and the largest symbols correspond to shifts of 60–80% from the means given in table 3*a*. Unlike figure 9, there is no obvious large-scale pattern in the measurements. This example is a combination of measurements for the modes ${}_0S_{21}$–${}_0S_{23}$.

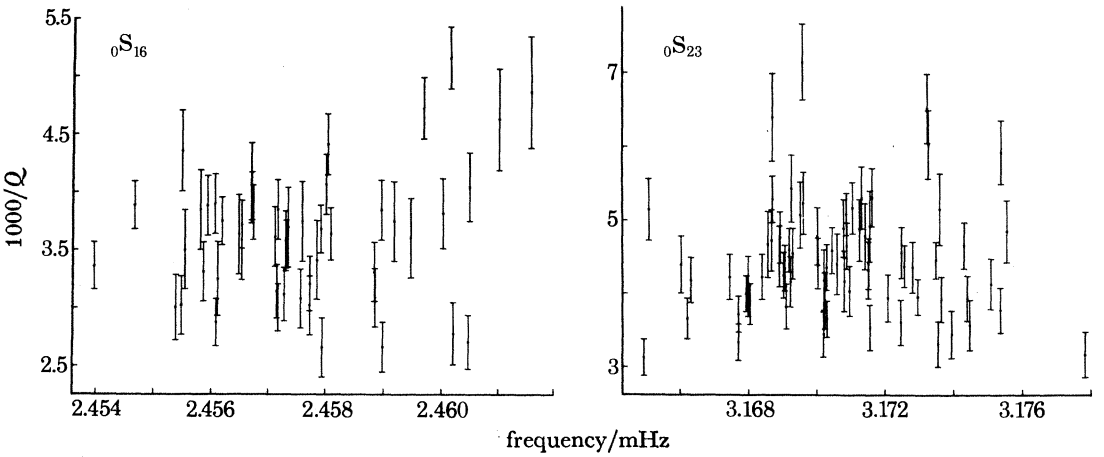

FIGURE 12. $1000/Q$ is plotted against frequency for the most accurate complex frequency measurements of ${}_0S_{16}$ and ${}_0S_{23}$. These diagrams illustrate the lack of correlation between centre frequency and apparent attenuation.

to a contribution to the apparent half width of a mode from lateral heterogeneity. The magnitude of such an effect is, as yet, unknown and complicates the assignment of errors to the mean Q values. In the absence of a better theory we have assumed that the scatter in the measured apparent Q values is caused by a random process and the error assigned in table 3 is assessed from the variance of the histograms shown in figure 8. We must also reluctantly conclude that lateral variations in anelasticity cannot be observed from raw measurements of the apparent Q of spectral lines, even when care is taken to reject measurements contaminated by splitting effects.

The mean Q values are plotted in figure 13 as a function of angular order. The smooth trend in the data is very pleasing but there are a few notable exceptions. These are the modes ${}_0S_{11}$, ${}_0S_{18}$ and ${}_0S_{19}$. We believe that the relatively high attenuation rates observed for these modes are a consequence of quasi-degenerate coupling (see for example Luh 1974; Woodhouse 1980). These observations should not be used in a modelling procedure that ignores this effect.

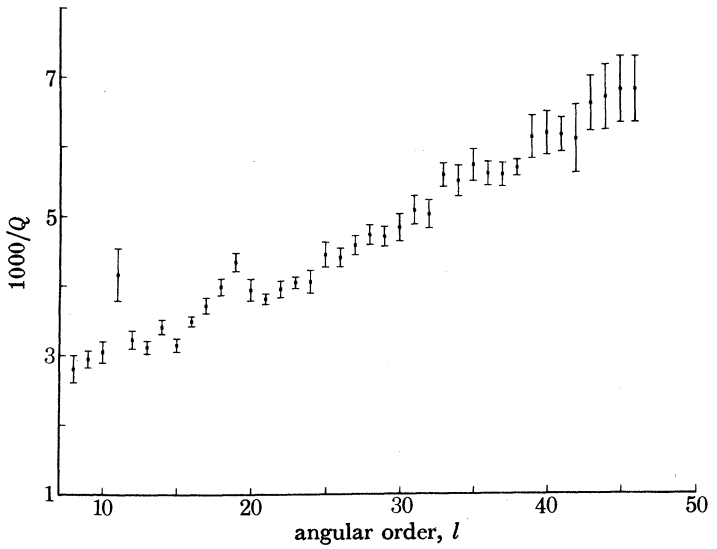

FIGURE 13. Means of the measurements of apparent attenuation of the fundamental modes ${}_0S_8$–${}_0S_{46}$.

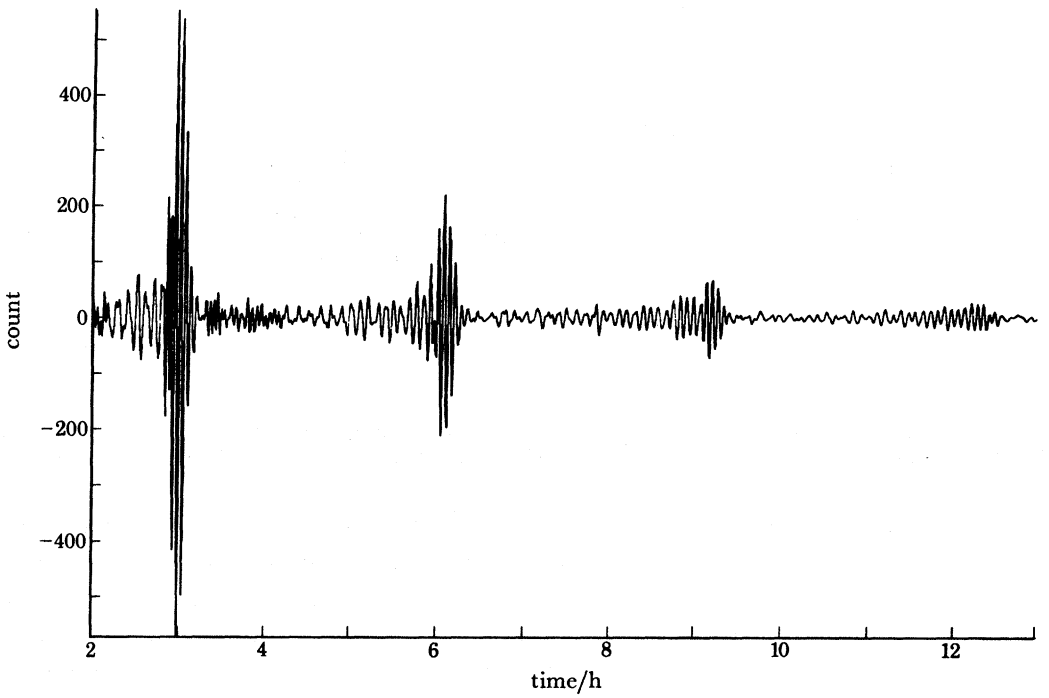

FIGURE 14. A record from the IDA station at College, Alaska (CMO; time origin: day 59 at 21 h 33 min 0 s) of an event 5° away. The Rayleigh wave pulses R_{23}, R_{45}, R_{67} and R_{89} are clearly visible.

We note from figure 9 that the distribution of pole positions is relatively dense though we have no near-equatorial paths as evidenced by the lack of poles for latitudes greater than 75°. The bias in our mean Q values due to inadequate sampling of the sphere should therefore be small. It is often thought that antipodal records give a good estimate of the mean properties of the Earth though it is well known that interference effects are serious for such records (Dahlen 1979). At low frequencies one can be effectively at the antipode at a distance of a few degrees and one record from the IDA network was within about 5° of an event giving it an antipodal character (figure 14). The low frequency spectrum is shown in figure 15 and most spectral peaks are obviously split.

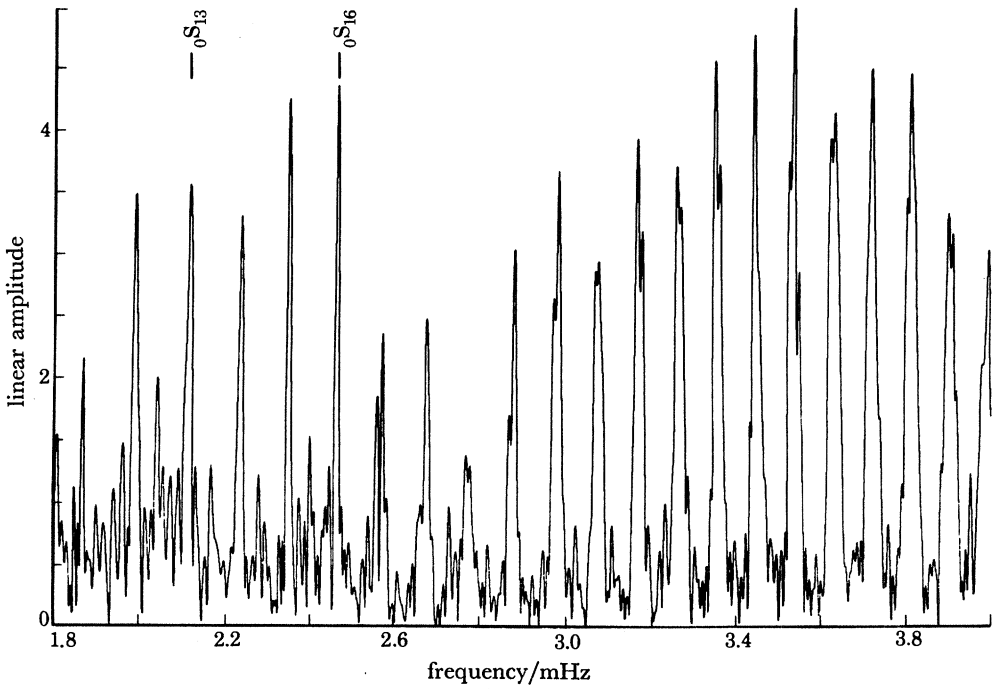

FIGURE 15. A linear amplitude spectrum of fifty hours of data from the record shown in figure 14. The fine-scale splitting of the fundamental modes above 2.5 mHz is very obvious.

Table 4 shows complex frequency measurements as a function of record length for two low frequency modes revealing that the observations are dominated by interference effects and the centre frequencies are anomalously high when compared with the mean measurements of table 3*a*. This result suggests that near-antipodal records are best avoided, at least when measuring modal parameters, if good estimates of the mean properties of the Earth are desired.

It turns out that the fundamental mode measurements presented in this section can be adequately fitted by very simple Q models so we have attempted to augment our data set with some overtone measurements. The number of isolated, well excited, singlet-like overtones is very small and a histogram analysis is possible on very few modes. The results of an attempt to do this are shown in table 3*b* and histograms of four overtones are presented in figure 16. The mean Q again show a sensible trend as a function of angular order for both the $_2$S group and the $_5$S group but the small number of measurements gives rather large uncertainties. We feel that more progress will be made by using singlet stacking procedures for modes of low angular order and high Q. Preliminary results from this work are given in table 3*c* along with other data taken from the literature. The Q values of $_0S_0$ and $_1S_0$ have been taken from Riedesel *et al.* (1980), these values

TABLE 4. COMPLEX FREQUENCY DETERMINATIONS FROM AN ANTIPODAL RECORD

mode	record length h	frequency mHz	Q
${}_0S_{13}$	25	2.1152	198
	35	2.1155	191
	45	2.1167	172
	55	2.1173	160
${}_0S_{16}$	25	2.4632	195
	35	2.4634	263
	45	2.4628	327
	55	2.4627	419

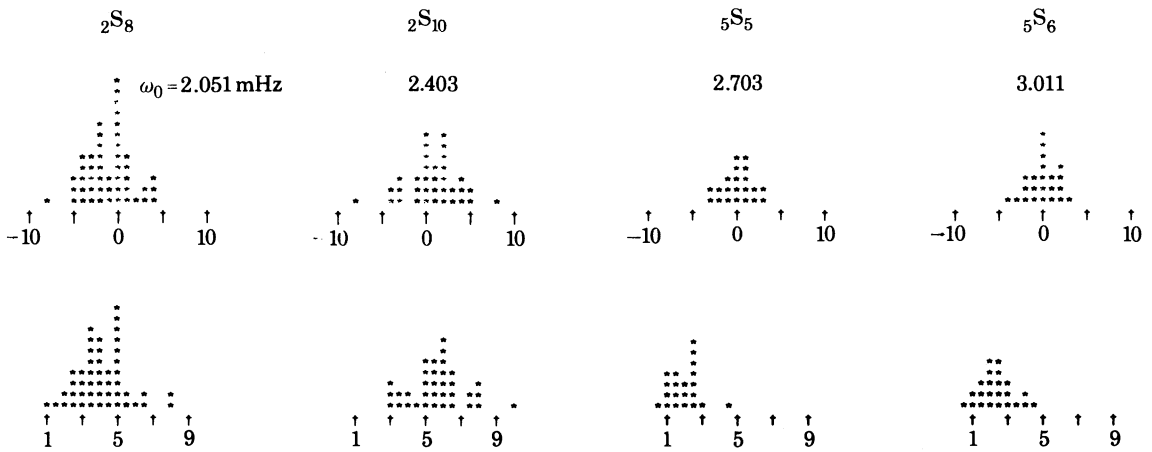

FIGURE 16. Histograms of apparent centre frequency and $1000/Q$ of four overtones. See legend to figure 8 for details.

have been confirmed by Chao (1981) using the a.r. method. The value for ${}_0S_0$ is similar to that of Knopoff *et al.* (1979) who used a shorter record. A single recording of the Colombian earthquake of 1970 provided the other radial mode measurements. The data were obtained by W. Farrell from a La Coste–Romberg gravimeter operating at Payson, Arizona. This record is unique; it is totally dominated by overtones with very high signal levels because of the depth and size of the event. Figure 17 illustrates demoded spectra of three of the radial modes. The signal level of ${}_4S_0$ exceeds that achieved by stacking IDA records from all the large events of the past 5 years. Stacking did, however, confirm the Q value for ${}_3S_0$, which is close to other highly excited overtones in the spectrum. Most of the spectral lines of overtones other than the radial modes are unresolvably split (figure 18) and give rise to spurious Q values. This fact does not seem to have been appreciated in previous analyses of this record (Sailor & Dziewonski 1978). In some cases the splitting is not obvious, for example ${}_8S_1$ appears to have a well-determined q of 1/715 but the modelling of the next section revealed that this is a biased measurement. This experience illustrates the danger of measuring Q from single records. Singlet stacking has been used for modes such as ${}_3S_1$; our results are similar to those of Chao & Gilbert (1980) for ${}_3S_1^{\pm 1}$ but ${}_3S_1^0$ is not well isolated by the stacking procedure giving a spuriously high Q value.

Table 3 constitutes the data set used in the inversions of the next section. It is our belief that very little other reliable modal Q data exist in the literature because of the lack of use of tapers in

most previous work and the relatively small amount of high quality data processed. It is clear from our results that measurements from individual records are subject to considerable scatter and it is only by analysing a large data set that good quality measurements are achieved. Fundamental mode attenuation has also often been measured by using travelling wave representations and it is interesting to note that our results are very similar to the results of Dziewonski & Steim (1982). The results of the next section show, however, that still greater precision is required to determine the detailed Q structure of the Earth.

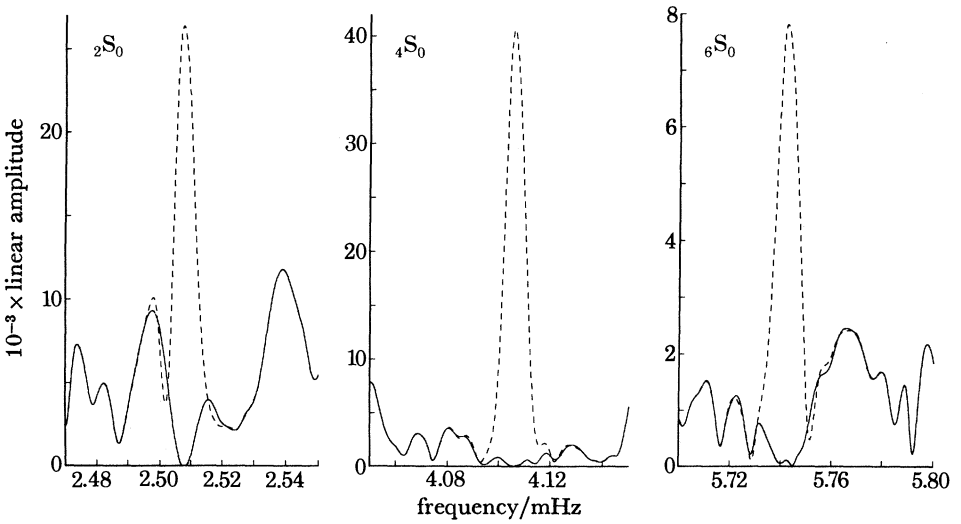

FIGURE 17. Demoded spectra of three radial modes from the Payson recording of the Colombian earthquake of 1970. The dashed line shows the original amplitude spectrum and the solid line shows the amplitude spectrum after the mode has been subtracted.

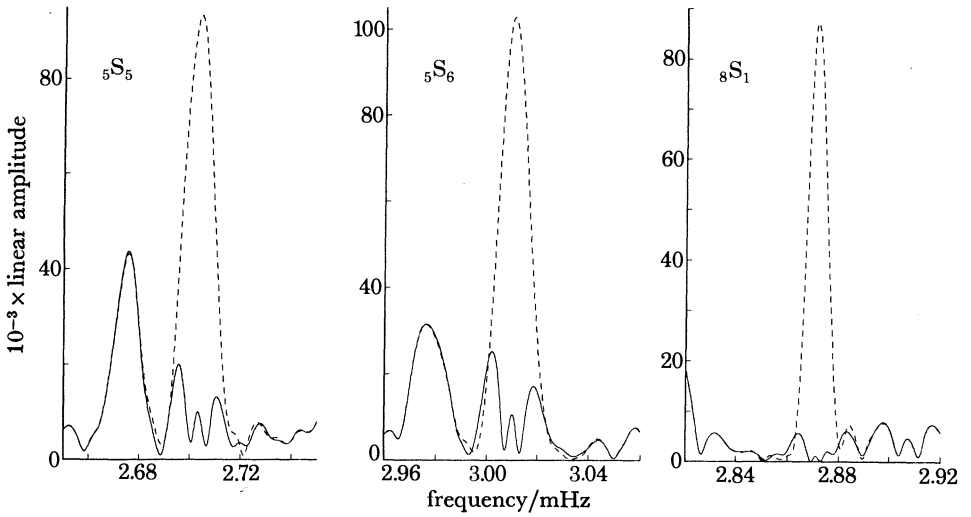

FIGURE 18. Demoded spectra of three high signal overtones from the Payson record. Two of these have large residual spectra. The mode $_5S_5$ has an apparent Q of about 350 and $_5S_6$ has an apparent Q of about 400. Both of these measurements are biased towards low values by the effects of splitting. The same also appears to be true of $_8S_1$ (see text).

4. Inversion and inference

The data in table 3 represent observed Q values for 71 spheroidal modes. There are 43 fundamental, ${}_0S_l$, modes, 7 radial, ${}_nS_0$, modes and 21 other overtone, ${}_nS_l$, modes, including 2 core modes (${}_6S_2$ and ${}_7S_3$) observed by Masters & Gilbert (1981). The assigned, relative standard deviations range from 2 % for some of the well observed fundamentals to 70 % for one of the core modes.

The observational procedures used to obtain the Q values permit us to invoke the diagonal sum rule (Gilbert 1971) in a statistical sense, and, thereby, to regard the observed attenuation data as belonging to the spherically averaged Earth. Accordingly, we seek radial models of $Q_\mu(r)$ and $Q_\kappa(r)$ to explain the data in table 3.

With an obvious notation we can write (6) in the form

$$\gamma_j = \int_0^1 G_j(r)\, q(r)\, \mathrm{d}r \quad (j = 1, \ldots, J), \tag{9}$$

where the data $\gamma_j = q_j$ in the first section. In finding solutions to (9) we want to account for errors in the data, represented by ϵ_j, and we must restrict ourselves to solutions for which

$$q(r) \geqslant 0, \tag{10}$$

i.e. the positivity constraint is met. Therefore, we are led to consider the existence, construction and evaluation of solutions to a linear inverse problem based on incomplete data (Parker 1980; Sabatier 1977). The positivity constraint (10) can be met either by linear programming (Luenberger 1973) or by the method of non-negative least squares (n.n.l.s.) (Lawson & Hanson, 1974).

As the results of this section may appear to be unduly pessimistic to anyone familiar with the detailed Q models that appear in the literature, we have performed an experiment with synthetic data that dramatically illustrates the poor resolution associated with modal Q measurements. Using the Q model in figure 19*a* and the eigenfunctions of model 1066A (Gilbert & Dziewonski 1975) we have computed Q values for the 200 lowest frequency ${}_nS_l$ modes excluding the Slichter mode ${}_1S_1$. In this data set there are 41 ${}_0S_l$ modes, $2 \geqslant l \geqslant 42$, the first 6 ${}_nS_0$ modes, and 153 ${}_nS_l$ overtones. The overtones include 19 core modes consisting of fluid–solid Stoneley modes and shear dominated overtones. Also present is the set of Stoneley modes for the core–mantle boundary (through ${}_2S_{23}$).

Our first step is to assess the information content of the synthetic data set of 200 Q values. To do this we assign $\sigma = 1$ % of each datum. Ranking and winnowing (Gilbert 1971) the data set, and using model 1066A, leads to an orthonormalized set of data functions $G_j(r)$ and a recombined set of q and σ values. These are the significant Earth data (s.E.d.) in the data set. There are 27 s.E.d. with $\sigma < 50$ % and 22 s.E.d. with $\sigma < 10$ %. Clearly, we cannot expect to infer much detail about the Q model with so few s.E.d. (It is instructive to recall that the 1066 gross Earth data used by Gilbert & Dziewonski (1975) had σ values ranging from 0.05 % to 0.4 %, and that they contained 222 s.E.d. with $\sigma < 100$ %.) Consequently, we shall confine our attention to models of homogeneous layers.

In (9) let $x_0 = 0$, $x_K = 1$ and define

$$G_{jk} = \int_{x_{k-1}}^{x_k} G_j(x)\, \mathrm{d}x \quad (k = 1, \ldots, K). \tag{11}$$

With q_k the constant value of q in the kth layer we have

$$\sum_{k=1}^{K} G_{jk} q_k = \gamma_j; \quad \text{standard deviation } \epsilon_j. \tag{12}$$

PHILOSOPHICAL TRANSACTIONS OF THE ROYAL SOCIETY A MATHEMATICAL, PHYSICAL & ENGINEERING SCIENCES

Solutions to (12) must satisfy $$q_k \geqslant 0, \tag{13}$$
the positivity constraint. We give each datum the same variance

$$\left.\begin{aligned} &\beta_j = \gamma_j \epsilon_j^{-1}, \quad H_{jk} = G_{jk}\epsilon_j^{-1}, \\ &\sum_{k=1}^{K} H_{jk} q_k = \beta_j; \quad \text{standard deviation 1.} \end{aligned}\right\} \tag{14}$$

We want to solve the problem

$$\text{minimize } \|Hq - \beta\| \text{ subject to } q \geqslant 0. \tag{15}$$

Expression (15) is problem n.n.l.s. (non-negative least squares) of Lawson & Hanson (1974, ch. 23). We solve it by using their algorithm n.n.l.s. The Euclidian norm of the residual vector is

$$\chi = \|Hq - \beta\| \tag{16}$$

and the relative misfit is ϵ where

$$\epsilon = \|Gq - \gamma\|/\|\gamma\|. \tag{17}$$

To assess the resolution of the data we have subdivided the model shown in figure 19*a* into 20 layers, 2 in the inner core, 3 in the outer core and 15 in the mantle. As a first experiment we allowed the 200 synthetic Q data to be accurate to five or six significant figures and, using the n.n.l.s. procedure, recovered the model shown in figure 19*b*. The agreement of q_μ with the original model is almost exact but q_κ shows significant fluctuations about the true value of 1/50 000 in the mid-mantle. Each datum is now replaced by a random number drawn from a population whose mean is the original datum and whose probability distribution is uniform from 0.99γ to 1.01γ and zero otherwise. This noisy, synthetic data set is used in all the following examples. Figure 19*c* shows the model derived from the noisy data by using the n.n.l.s. procedure. There are nine layers for which $q_\kappa = 0$. This result illustrates the fundamental theorem of linear programming (Luenberger 1973), which states that, when H in (14) has rank $L = K$, if there is any set of q satisfying (15), there must be a set in which *at most* L of them are non-zero and the rest vanish. If we increase the number of layers, K, then we shall eventually have $L < K$. The model will approach a δ-function model of the sort discussed by Parker (1980) and some layers will have no attenuation. The model in figure 19*c* does not represent numerical instability or poor data. It represents the effect of the positivity constraint. A geometrical interpretation of the foregoing remarks, including the case $L < K$, may be found in the discussion of Lawson & Hanson (1974, pp. 159–160) of the Kuhn–Tucker theorem.

Although the two models derived from synthetic data are considerably different they have very nearly the same average value of q_μ in the mantle. This is not a surprising result. It has been a central theme in the theory of geophysical inverse problems for the past 15 years that certain average features of the Earth can be determined even though details of structure remain unknown.

Averaging is a smoothing operation. Before we discuss how we obtain linear averages of the model we discuss simple smoothing methods. First we reduce the number of layers in the model to be exactly the same as that in the original model for q_μ. For the real Earth we cannot do this; we merely use it to illustrate one kind of smoothing. The n.n.l.s. procedure with 200 noisy data yields the model in figure 20*a*. In the upper mantle q_κ is recovered and q_μ is nearly correct in both the mantle and the inner core.

While this example is unrealistic in the sense that we do not know how to assign thick layers to a realistic model, it is instructive in that it shows how apparent resolution is affected by a particular parametrization.

PHILOSOPHICAL TRANSACTIONS OF THE ROYAL SOCIETY A MATHEMATICAL, PHYSICAL & ENGINEERING SCIENCES

Another kind of smoothing comes from the observation that q_μ tends to increase with r above the zone of high q_μ at the base of the mantle. In any region we can attempt to force the observed behaviour to take place as follows. In a shell of N layers change variables

$$\left.\begin{aligned} &d_1 = q_1, \quad d_n = q_n - q_{n-1} \quad (n = 2, \ldots, N), \\ &d = Dq, \quad q = D^{-1}d = Sd. \end{aligned}\right\} \tag{18}$$

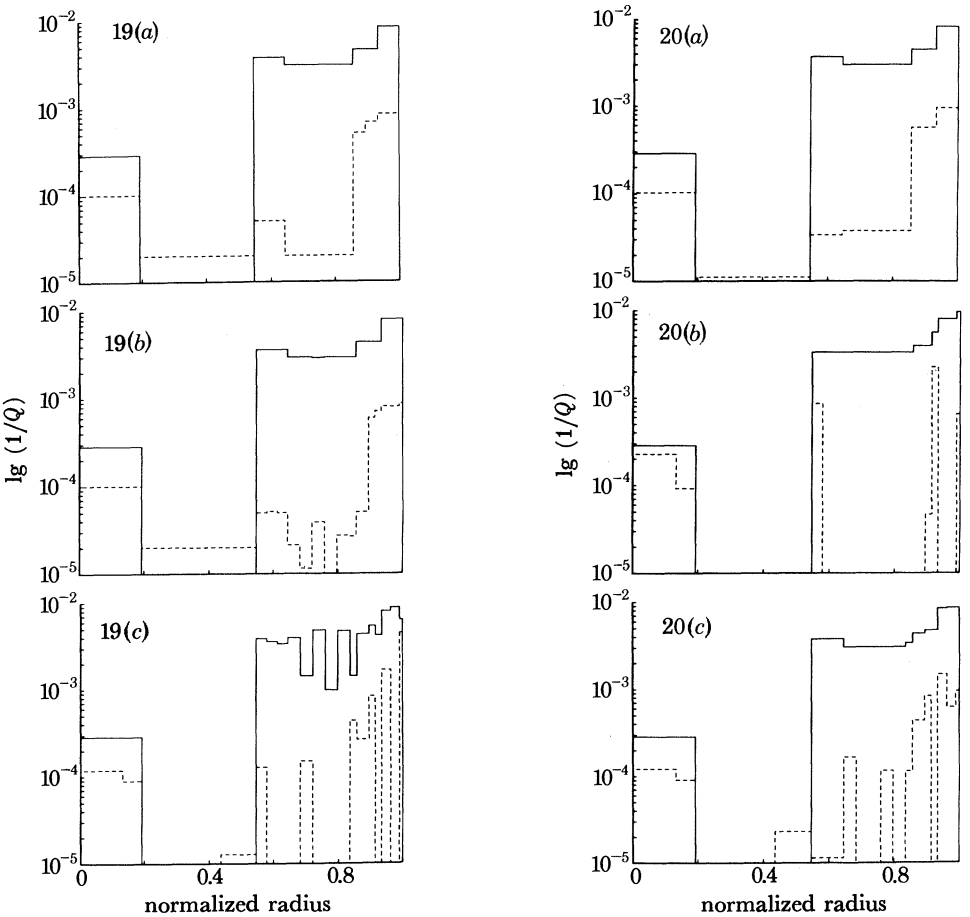

FIGURE 19. (*a*) A q model used to generate synthetic data. In this diagram, and in figures 20, 22 and 23, the solid line shows the q_μ structure and the dashed line the q_κ structure. The horizontal axis extends from the centre of the Earth ($r = 0$) to the surface ($r = 1$). The average q_μ in the mantle is 1/238. (*b*) A 20 layer q model constructed, by using the n.n.l.s. procedure, from 200 synthetic data accurate to six significant figures. Even with this precision q_κ shows some oscillatory behaviour in the mantle. The average q_μ in the mantle is 1/238. (*c*) A 20 layer q model constructed, by using the n.n.l.s. procedure, from 200 synthetic data with 1% noise added. q_κ now exhibits some δ-function behaviour (see text) and q_μ is no longer accurately recovered. χ and ϵ, defined by equations (16) and (17) in the text, are 7.95 and 0.56% respectively. The average q_μ in the mantle is 1/240.

FIGURE 20. The effect of various smoothing operations on model retrieval from 200 noisy synthetic data. (*a*) A six-layer q model constructed by using the n.n.l.s. procedure. χ is 8.3, ϵ is 0.59% and the average q_μ in the mantle is 1/238. (*b*) A 20 layer model with q_μ constrained to be a monotonically increasing function of radius in the inner core and mantle and q_κ constrained to be positive. χ is 24.8, ϵ is 1.76% and the average q_μ in the mantle is 1/235. (*c*) As in figure 20*b*, but with allowance for a zone of high q_μ at the base of the mantle. χ is now 8.1, ϵ is 0.57% and the average q_μ in the mantle is 1/238.

In (18) D is a first difference matrix and its inverse S is a smoothing matrix. We want to solve the problem

$$\text{minimize } \|Hq-\beta\| = \|HSd-\beta\| \text{ subject to } d \geqslant 0. \tag{19}$$

The constraint $d \geqslant 0$ forces q to increase, or at least to be monotonic, with n. With the constraint (19) the δ-function model will be a model of d. The model of q will consist of steps. Requiring $q_\kappa \geqslant 0$ and applying the above procedure to q_μ in both the mantle and the core we obtain the model shown in figure 20*b*.

There are only two major steps in q_μ in the mantle. The largest relative misfit between data and computed values occurs for the Stoneley mode ${}_2S_{23}$. For ${}_2S_{23}$ the synthetic value of Q is 363, the noisy synthetic value is 360 and the computed value for figure 23 is 382, a misfit of 5.8 %.

It is often stated that observations of Stoneley modes on the core–mantle boundary will constrain Q structure at the base of the mantle. Comparing figures 19*a* and 20*b* we have two models, the former having a low Q_μ zone at the base of the mantle, 20 % lower than the mid-mantle value, and the latter having a constant Q_μ for nearly 2000 km above the core–mantle boundary. Yet, the greatest difference in computed Q values is only 5.8 %, and that for a mode unlikely to be observed. In the example above, if we had used $\sigma = 5$ % rather than $\sigma = 1$ % then $\chi = 5$ and the largest misfit for ${}_2S_{23}$, would have been acceptable. The example illustrates the accuracy required of attenuation data to permit useful geophysical inferences to be made.

If the flat q_μ in figure 20*b* makes one suspect a zone of high q_μ at the bottom of the mantle then another change of variables in (18) can be made to allow such a feature:

$$d_1 = q_1, \quad d_2 = q_1 - q_2, \quad d_n = q_n - q_{n-1} \quad (n = 3, \ldots, N). \tag{20}$$

The constraint $d \geqslant 0$ allows $q_1 \leqslant q_2$ and forbids $q_1 > q_2$. Thereafter q is a monotonically increasing function of n. This change in modelling leads to the model in figure 20*c* (q_μ is now in close agreement with the originating model).

Obviously, there are endless variations on (18) for deriving smooth models with or without zones of high or low q_μ or q_κ. It is encouraging that average q_μ in the mantle seems to be a stable quantity in the models derived from the 200 synthetic data and it is further encouraging that the δ-functions in d, steps in q, are in, or close to, the right radii. However, with a sufficiently large number of layers, numerical experiments show that spikes in d can be relocated with only mild changes in χ. Thus we are led to consider other forms of smoothing and of inference.

Let us return to (9) and assume that the data have been ranked and winnowed:

$$\int_0^1 G_j(x)\, G_k(x)\, \mathrm{d}x = \delta_{jk}. \tag{21}$$

To determine the average value of $q(x)$ between x_1 and x_2 we want to find

$$\bar{q} = (x_2 - x_1)^{-1} \int_{x_1}^{x_2} q(x)\, \mathrm{d}x. \tag{22}$$

Let
$$B(x) = (x_2 - x_1)^{-1}[H(x-x_1) - H(x-x_2)]. \tag{23}$$

$B(x)$ is zero outside the interval (x_1, x_2), is constant inside the interval and has unit area. In (9) we seek a linear combination of $G_j(x)$ to approximate $B(x)$ by the averaging function

$$A(x) = \sum_{j=1}^{J} a_j G_j(x). \tag{24}$$

If $A(x) = B(x)$ we have from (22), (23), (24) and (9)

$$\sum_{j=1}^{J} a_j \gamma_j = \bar{q}. \tag{25}$$

Note that the average, $\bar{q}$, is constructed without reference to a model of q. This is a very important feature of linear inverse problems. Linear averages of the solution can be constructed as linear combinations of the data without a model being known (Backus & Gilbert 1968). The variance associated with (25) is

$$\nu = \sum_{j=1}^{J} a_j^2 \epsilon_j^2. \tag{26}$$

We want to minimize $\|B(x) - A(x)\|$ and ν and we want $A(x)$ to have unit area. This is a standard resolving power calculation (Backus & Gilbert 1970). Let

$$g_j = \Delta^{-1} \int_{x_1}^{x_2} G_j(x)\, \mathrm{d}x, \quad \Delta = x_2 - x_1. \tag{27}$$

Then, using the summation convention gives

$$\|B(x) - A(x)\|^2 = \mu = a_j a_j - 2 a_j g_j + \Delta^{-1}. \tag{28}$$

The constraint of unit area for $A(x)$ is met by introducing

$$h_j = \int_0^1 G_j(x)\, \mathrm{d}x, \quad a_j h_j = 1. \tag{29}$$

The calculation is summarized as follows.

$$\text{Minimize } \mu \cos\theta + \omega\nu \sin\theta \text{ subject to } a_j h_j = 1 \tag{30}$$

for $0 \leqslant \theta \leqslant \frac{1}{2}\pi$ with ω a weighting factor chosen to balance the calculation. The solution for a_j is

$$\left.\begin{aligned} &d_j = \cos\theta + \epsilon_j^2 \sin\theta, \quad f_j = h_j/d_j, \quad b_j = \cos\theta\, g_j/d_j, \\ &\lambda = (1 - b_j h_j)/(f_j h_j), \quad \text{summation implied}, \quad a_j = b_j + \lambda f_j. \end{aligned}\right\} \tag{31}$$

Since the constraint $a_j h_j = 1$ makes $A(x)$ unimodular, $\Delta a_j g_j$ is the area of $A(x)$ in the interval (x_1, x_2) and $1 - \Delta a_j g_j$ is the spill-over into other intervals. As θ increases, μ increases and ν decreases. The area $A(x)$ deteriorates as an approximation to $B(x)$ and falls outside (x_1, x_2). The spill-over $1 - \Delta a_j g_j$ usually increases.

Inspection of (6) shows that the data depend upon two independent functions of radius, $q_\kappa(r)$ and $q_\mu(r)$. Backus & Gilbert (1968) show how a generalized definition of the inner product can be used to explore further trade-offs among error, spill-over, variations from $B(x)$ in (23), etc. This degree of sophistication is not warranted with the number of s.E.d. available to us and the multi-dimensionality of the inverse problem (6) is handled by simply redefining (9):

$$\gamma_j = \int_0^2 G_j(r)\, q(r)\, \mathrm{d}r,$$

where $$G_j(r) = K_j(r), \quad q(r) = q_\kappa(r) \quad (0 \leqslant r \leqslant 1),$$

and $$G_j(r) = M_j(r-1), \quad q(r) = q_\mu(r-1) \quad (1 < r \leqslant 2).$$

The analysis of resolving power in intervals, presented above, has been applied to the 27 s.E.d. derived from the 200 noisy, synthetic data. In the first of two numerical experiments we have chosen the inner core and the mantle as the intervals.

For q_κ in the inner core the minimum spill-over at $\theta = 0$ is 0.214. However, the error ($\epsilon = \nu^{\frac{1}{2}}$) is 3.4 relative to $q_\kappa = 1/11\,600$. Increasing μ slightly, to a spill-over of 0.215 gives a $\sigma = 5.6\,\%$ relative to $q_\kappa = 1/2000$ where $\sigma = \epsilon/q$ is relative error. Obviously, $A(x)$ is not a good averaging function and the spill-over has biased q_κ to a large value (Q_κ to a small value) in the inner core. In the mantle, estimates of q_κ range from 1/3000 (spill-over = 0.023, $\sigma = 4.5\,\%$) to 1/2000 (spill-over = 0.073, $\sigma = 2.4\,\%$). The mean value of q_κ in the mantle for the model in figure 19 is 1/4407. Again the average is biased by spill-over into intervals of high q (q_μ in this case). The averaging function $A(x)$ for $\sigma = 4.5\,\%$ is shown in figure 21*a*.

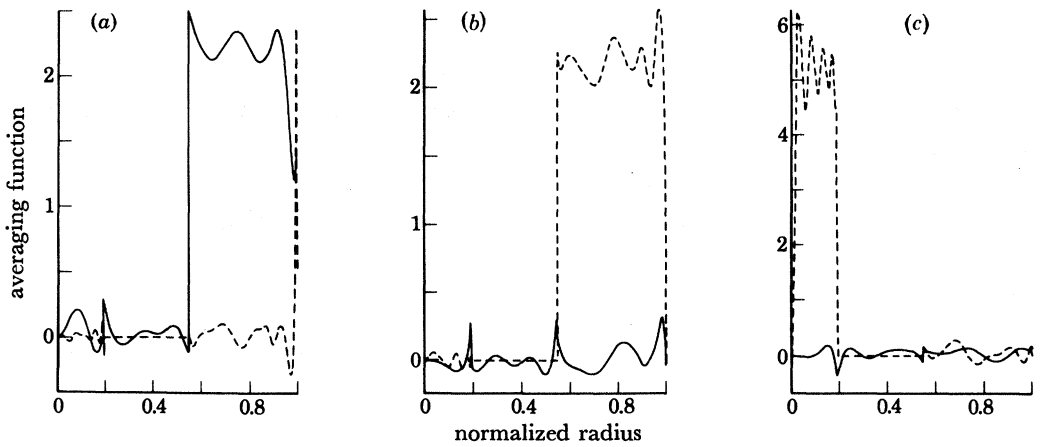

FIGURE 21. Boxcar-like averaging functions constructed by using 200 noisy synthetic data. The solid line shows the averaging function in regions of bulk dissipation and the dashed line shows the averaging function in regions of shear dissipation. The optimum averaging functions for (*a*) q_κ in the mantle, (*b*) q_μ in the mantle and (*c*) q_μ in the inner core are shown.

For q_μ in the inner core the minimum spill-over is 0.062 and $\sigma = 2.2\,\%$ relative to $q_\mu = 1/2440$. The small spill-over into mantle intervals of large q_μ (small Q_μ) biases our averages of q_μ in the inner core. In the mantle, estimates of q_μ range from 1/241 (spill-over = 0.008, $\sigma = 0.2\,\%$) to 1/242 (spill-over = 0.013, $\sigma = 0.16\,\%$). In figure 21*b* we have $A(x)$ for the latter point on the trade-off curve. It is a very good approximation to $B(x)$ and average q_μ differs only slightly from 1/238, the value for the model in figure 19*a*.

The foregoing analysis shows that, with accurate, slightly noisy data, we can obtain good average values of q_μ in the mantle. For q_κ, and for q_μ in the inner core, the results are biased. To bias a large q with a small amount of small q does not cause a serious effect, but to bias a small q with a small amount of large q can have a very serious effect. For this reason q_κ will always be much less well determined than q_μ.

In the second example of resolving power analysis we have chosen the five intervals for q_μ in figure 19*a*. We shall refer to these intervals as layer 1 to layer 5. The model q_μ values in them are 1/3500, 1/270, 1/330, 1/220, 1/120. Typical averages are given in the form (layer n, q_μ, spill-over, σ): (1, 1/2740, 0.066, 2 %), (2, 1/273, 0.075, 1.1 %), (3, 1/324, 0.064, 0.56 %), (4, 1/219, 0.12, 0.98 %), (5, 1/129, 0.11, 0.42 %). These results for q_μ are quite good although q_μ in the inner core is biased by the spill-over of 0.066 into the mantle where q_μ is large. The best $A(x)$ for q_μ in the inner core is shown in figure 21*c*.

PHILOSOPHICAL TRANSACTIONS OF THE ROYAL SOCIETY A MATHEMATICAL, PHYSICAL & ENGINEERING SCIENCES

The analysis of resolving power in intervals suggests a discretized version of the usual treatment of linear inverse problems. We return to (12) and assume that the G_{ik} are orthonormal:

$$G_{ik}G_{jk} = \delta_{ij} \tag{32}$$

(i.e. that ranking and winnowing has been done). In this case the number of s.E.d. cannot exceed the number of parameters q_k. We seek a linear combination of G_{jk} that approximates the Kronecker δ for one of the parameters. Our goal is to have

$$a_j G_{jk} = \delta_{kl} \tag{33}$$

for the lth parameter. Equation (33) represents the ideal and in fact we shall have an averaging vector

$$a_j G_{jk} = A_k. \tag{34}$$

From (12)

$$a_j \gamma_j = a_j G_{jk} q_k = A_k q_k = \bar{q}. \tag{35}$$

If $A_k = \delta_{kl}$, $\bar{q} = q_l$. The variance associated with (35) is given by (28). We want to minimize the difference between A_k and δ_{kl}

$$\mu = \sum_k (A_k - \delta_{kl})^2 = \sum_j (a_j - G_{jl})^2. \tag{36}$$

We also impose the constraint $a_j h_j = 1$ where

$$h_j = \sum_k G_{jk}, \quad a_j h_j = 1. \tag{37}$$

If we let

$$g_j = G_{jl} \tag{38}$$

the solution is given by (31). For a given l, $a_j = G_{jl}$ for $\theta = 0$ and $A_k = \delta_{kl}$. As θ increases, μ increases, ν decreases and A_k deteriorates as an approximation to δ_{kl}. The r.m.s. ripple of A_k about δ_{kl} is $(\mu/K)^{\frac{1}{2}}$ for K parameters. This will simply be termed the ripple.

In using discretized resolving power one is effectively asserting that a particular parametrization is acceptable for a given problem. The assertion greatly simplifies the problem. Instead of forming linear averages of an unknown function, as in the foregoing interval analysis, one forms linear averages of a few discrete parameters that are asserted to be appropriate. We expect the discretized resolving power analysis to provide superior results to the interval analysis because of the additional information provided by the asserted parametrization.

We have confined our attention to q_μ and have chosen the parametrization in figure 19*a*. There are 11 parameters, 6 for q_κ and 5 for q_μ. For q_μ we construct trade-off curves in the traditional way for each of the five layers. In each case the data are good enough to allow us to accept the end-point, $\theta = 0$. At this point there is no ripple. The results are (layer n, q_μ, σ): (1, 1/3760, 0.3 %), (2, 1/270, 0.4 %), (3, 1/331, 0.4 %), (4, 1/222, 0.8 %), (5, 1/121, 0.34 %). In these examples a slight decrease in ν from its maximum value leads to a rapid increase in ripple.

The results for discretized resolving power show that a good choice of parametrization and a large number of slightly noisy data can lead to very good results. It must be emphasized that the improvement comes from the assertion of a correct structure.

With the results of the numerical experiments on 200 synthetic data ($\sigma = 1$ %) in mind, we now turn to the interpretation of the 71 observed data in table 3. Ranking and winnowing the 71 observed data gives us 20 s.E.d. for $\sigma \leqslant 50$ % and 5 s.E.d. for $\sigma \leqslant 10$ %. The s.E.d. are clustered towards large values; 11 s.E.d. have 50 % $\geqslant \sigma \geqslant$ 40 %. This is a sobering outcome. We have 1/10 the s.E.d. of Gilbert & Dziewonski (1975) with which to make inferences. Our models will certainly be coarser than theirs. Resolvable features will be few and large.

First we apply (15) to the 71 data. Using a model of 20 layers, 37 parameters, we obtain the result shown in figure 22*a*. In table 5 we compare computed with observed Q values. Given the over-parametrization evident in the model, and its δ-function structure, we conclude that table 5 exhibits some outliers in the data. The modes ${}_0S_{11}$ and ${}_0S_{19}$ are almost certainly contaminated by

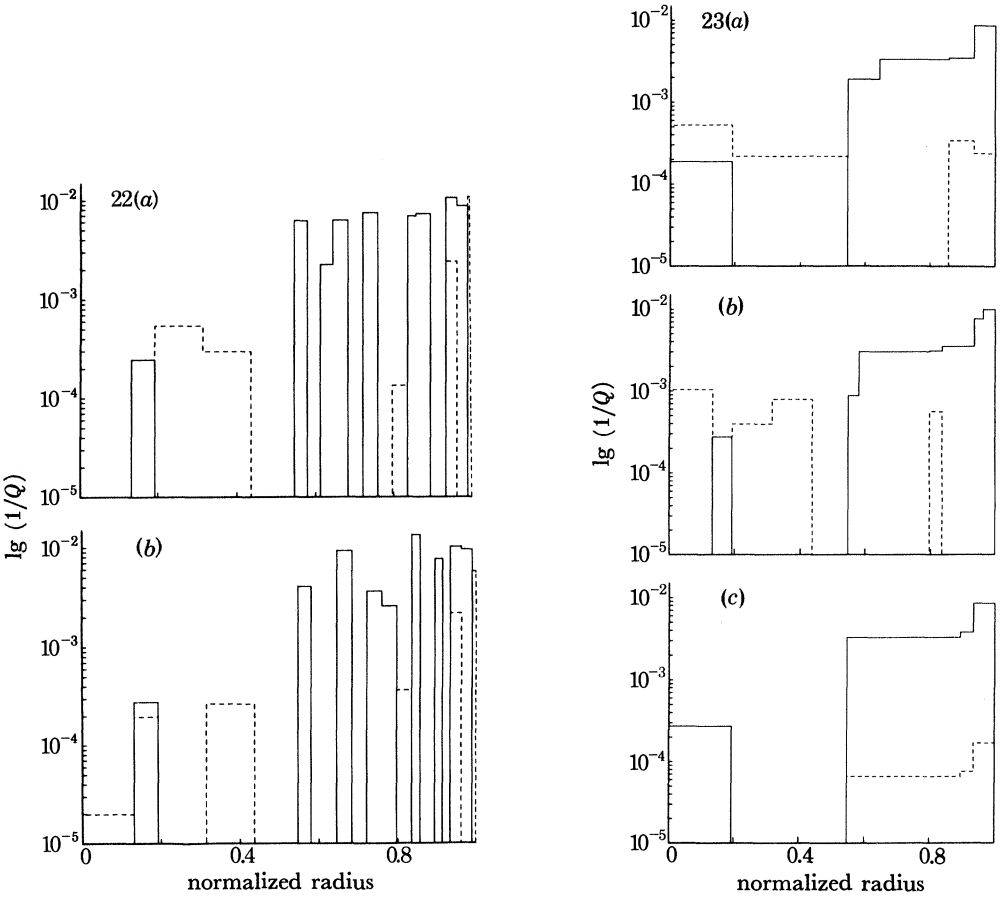

FIGURE 22. Twenty-layer models constructed from the observed data by using the n.n.l.s. procedure with no smoothing constraints. (*a*) A model derived from all 71 data. χ is 9.3, ϵ is 4.8% and the average q_μ in the mantle is 1/256. (*b*) A model derived from the data after removal of nine outliers. χ is now 5.6, ϵ is 3.0% and the average q_μ in the mantle is 1/264. Both these models show the δ-function structure associated with over-parametrization in conjunction with the positivity constraint.

FIGURE 23. The effect of various smoothing operations on model retrieval, obtained by using 62 observed data. (*a*) A six-layer q model constructed by using the n.n.l.s. procedure. χ is 6.0, ϵ is 3.2% and the average q_μ in the mantle is 1/264. (*b*) A 20 layer q model with q_μ constrained to be a monotonically increasing function of radius in the inner core and mantle and q_κ constrained to be positive. χ is 5.8, ϵ is 3.1% and the average q_μ in the mantle is 1/259. (*c*) A five-layer q model constructed with the constraint that $q_\mu \geqslant 50q_\kappa$. χ is 7.0, ϵ is 3.7% and the average q_μ in the mantle is 1/245.

the effects of resonant coupling. The modes ${}_8S_1$ and ${}_{13}S_1$ were measured from only one or two records and the measurements are probably contaminated by beating between the ± 1 singlets. The mode ${}_0S_3$ was measured from a single South Pole record with a low s.n.r. and is obviously a suspect observation. A second application of (15) shows that a few outliers remain. At this stage the modes ${}_0S_5$, ${}_0S_{18}$, ${}_2S_0$ and ${}_3S_2$ are rejected. Remaining are 62 data including the two core modes ${}_6S_2$ and ${}_7S_3$. Separately, neither core mode is well fitted, and each could be rejected as an outlier.

TABLE 5. COMPARISON OF THE OBSERVED Q DATA WITH THE Q VALUES COMPUTED FROM THE MODEL IN FIGURE 22a

mode	observed Q	model Q	difference (%)	s.d. (%)
${}_0S_3$	300	401	25.2	28.0
${}_0S_4$	391	361	−8.2	23.0
${}_0S_5$	306	348	12.0	7.0
${}_0S_7$	345	341	−1.3	7.0
${}_0S_8$	356	338	−5.2	7.0
${}_0S_9$	340	335	−1.5	4.0
${}_0S_{10}$	328	330	0.7	5.0
${}_0S_{11}$	241	324	25.7	9.0
${}_0S_{12}$	311	317	2.0	4.0
${}_0S_{13}$	321	310	−3.7	3.0
${}_0S_{14}$	294	302	2.5	3.0
${}_0S_{15}$	318	294	−8.3	3.0
${}_0S_{16}$	287	286	−0.4	2.0
${}_0S_{17}$	269	279	3.5	3.0
${}_0S_{18}$	251	272	7.7	3.0
${}_0S_{19}$	231	265	12.9	3.0
${}_0S_{20}$	254	259	2.0	4.0
${}_0S_{21}$	263	253	−3.8	2.0
${}_0S_{22}$	253	248	−2.1	3.0
${}_0S_{23}$	248	242	−2.4	2.0
${}_0S_{24}$	247	237	−4.3	4.0
${}_0S_{25}$	225	231	2.7	4.0
${}_0S_{26}$	227	226	−0.5	3.0
${}_0S_{27}$	219	221	0.7	3.0
${}_0S_{28}$	212	215	1.6	3.0
${}_0S_{29}$	213	210	−1.3	3.0
${}_0S_{30}$	207	205	−0.9	4.0
${}_0S_{31}$	197	200	1.6	4.0
${}_0S_{32}$	199	196	−1.8	4.0
${}_0S_{33}$	179	191	6.3	3.0
${}_0S_{34}$	182	187	2.5	4.0
${}_0S_{35}$	175	182	4.1	4.0
${}_0S_{36}$	179	179	−0.3	3.0
${}_0S_{37}$	179	175	−2.4	3.0
${}_0S_{38}$	176	171	−2.8	2.0
${}_0S_{39}$	163	168	2.9	5.0
${}_0S_{40}$	162	165	1.7	5.0
${}_0S_{41}$	162	162	−0.1	4.0
${}_0S_{42}$	164	159	−3.0	8.0
${}_0S_{43}$	151	157	3.6	6.0
${}_0S_{44}$	149	154	3.4	7.0
${}_0S_{45}$	147	152	3.3	7.0
${}_0S_{46}$	147	150	2.0	7.0
${}_0S_0$	5700	5690	−0.2	5.0
${}_1S_0$	1850	1842	−0.4	12.0
${}_2S_0$	1800	1620	−11.1	25.0
${}_3S_0$	1410	1398	−0.9	10.0
${}_4S_0$	1215	1204	−0.9	5.0
${}_5S_0$	1250	1202	−4.0	10.0
${}_6S_0$	1150	1405	18.1	17.0
${}_3S_1$	900	810	−11.2	11.0
${}_8S_1$	715	1026	30.3	15.0
${}_{13}S_1$	660	1026	35.7	15.0
${}_3S_2$	440	559	21.3	25.0
${}_5S_2$	315	348	9.5	10.0
${}_6S_2$	2900	2295	−26.4	70.0

PHILOSOPHICAL TRANSACTIONS OF THE ROYAL SOCIETY A MATHEMATICAL, PHYSICAL & ENGINEERING SCIENCES

TABLE 5. (*cont.*)

mode	observed Q	model Q	difference (%)	s.d. (%)
${}_{10}S_2$	1080	983	−9.8	10.0
${}_{13}S_2$	1025	998	−2.7	10.0
${}_{1}S_3$	340	300	−13.5	15.0
${}_{2}S_3$	541	449	−20.5	18.0
${}_{5}S_3$	339	315	−7.7	17.0
${}_{7}S_3$	2800	3869	27.6	60.0
${}_{1}S_4$	297	291	−2.2	23.0
${}_{5}S_4$	457	531	14.0	22.0
${}_{5}S_5$	511	543	5.9	24.0
${}_{2}S_6$	235	253	7.2	18.0
${}_{5}S_6$	501	541	7.4	15.0
${}_{5}S_7$	479	519	7.7	29.0
${}_{2}S_8$	227	216	−5.3	7.0
${}_{2}S_{10}$	193	200	3.6	10.0
${}_{2}S_{12}$	189	193	2.3	15.0

Together they contribute 1 s.E.d. that splits the difference between them. That is, taken alone, they provide 1 s.E.d. with $\sigma = 46\,\%$ and another linear combination of their data that is statistically irrelevant. We retain them as data because of their apparent sensitivity to Q_μ in the inner core.

We have ranked and winnowed the 62 data and find 9 s.E.d. for $\sigma \leqslant 50\,\%$ and 5 s.E.d. for $\sigma \leqslant 10\,\%$. The fact that there are now fewer s.E.d. is offset by the fact that we have lost only the inaccurate s.E.d. in rejecting outliers. The 62 data with 9 s.E.d. are our basic data set for investigating Q structure.

An application of (15) leads to the δ-function model in figure 22*b*. In table 6 we compare computed and observed Q values. There are no outliers in the data. With the over-parametrized 20 layer model we constrain $q_\kappa = 0$, and apply the n.n.l.s. procedure to (15). The resulting model, still δ-like in q_μ, has $\chi = 7.9$, $\epsilon = 4.6\,\%$ and average mantle $q_\mu = 1/240$. The radial modes are poorly fitted; all have values of attenuation that are too low. For example, the fundamental radial mode, ${}_0S_0$, has computed $q = 1/7260$ about 27 % lower than the observed value $1/5700 \pm 5\,\%$. Since the model is still over-parametrized we conclude that $q_\kappa > 0$ somewhere in the Earth. This conclusion is in agreement with Sailor & Dziewonski (1978) and Anderson & Hart (1978).

To obtain a smoother model we choose the six-layer structure in figure 19*a*. Applying (15) gives the model in figure 23*a*. In the inner core q_μ is small but the two core modes are still reasonably well fitted. The high value of q_κ accounts for this. In the mantle q_μ increases monotonically with r. This suggests that it is appropriate to apply (18) and (19) as a modelling procedure. Using the 20 layer structure, requiring $q_\kappa \geqslant 0$ and applying (18) and (19) to q_μ in both the inner core and the mantle gives the model in figure 23*b*. In the inner core q_κ is very low; q_μ is larger and provides the attenuation in that region. The fit to the two core modes is unchanged. In fact there is little to choose between the two models. In the one smoothed by inversion for first differences there are only two major steps in q_μ in the mantle plus a thin zone of low q_μ (high Q_μ) at the base of the mantle.

On physical grounds we can argue that $q_\mu > q_\kappa$ in solids. Heinz *et al.* (1982) predict $q_\mu \approx 100\, q_\kappa$ for typical mineral assemblages of the mantle, based on viscoelastic theory. Their calculated values of q_μ/q_κ for their assumed mineral assemblages are well within the range suggested by recent Earth models, e.g. model PREM of Dziewonski & Anderson (1981). We can either constrain

Table 6. Comparison of the observed Q data with the Q values computed from the model in figure 22*b*

mode	observed Q	model Q	difference (%)	s.d. (%)
${}_0S_4$	391	395	1.1	23.0
${}_0S_7$	345	356	3.0	7.0
${}_0S_8$	356	348	−2.4	7.0
${}_0S_9$	340	339	−0.3	4.0
${}_0S_{10}$	328	331	0.9	5.0
${}_0S_{12}$	311	317	1.9	4.0
${}_0S_{13}$	321	310	−3.4	3.0
${}_0S_{14}$	294	304	3.3	3.0
${}_0S_{15}$	318	298	−6.8	3.0
${}_0S_{16}$	287	291	1.5	2.0
${}_0S_{17}$	269	285	5.6	3.0
${}_0S_{20}$	254	266	4.4	4.0
${}_0S_{21}$	263	259	−1.5	2.0
${}_0S_{22}$	253	253	−0.2	3.0
${}_0S_{23}$	248	246	−0.9	2.0
${}_0S_{24}$	247	239	−3.2	4.0
${}_0S_{25}$	225	233	3.4	4.0
${}_0S_{26}$	227	227	−0.1	3.0
${}_0S_{27}$	219	221	0.7	3.0
${}_0S_{28}$	212	215	1.3	3.0
${}_0S_{29}$	213	209	−1.8	3.0
${}_0S_{30}$	207	204	−1.5	4.0
${}_0S_{31}$	197	199	0.9	4.0
${}_0S_{32}$	199	194	−2.5	4.0
${}_0S_{33}$	179	190	5.6	3.0
${}_0S_{34}$	182	185	1.8	4.0
${}_0S_{35}$	175	181	3.6	4.0
${}_0S_{36}$	179	178	−0.7	3.0
${}_0S_{37}$	179	174	−2.7	3.0
${}_0S_{38}$	176	171	−2.9	2.0
${}_0S_{39}$	163	168	3.0	5.0
${}_0S_{40}$	162	165	2.0	5.0
${}_0S_{41}$	162	163	0.4	4.0
${}_0S_{42}$	164	160	−2.4	8.0
${}_0S_{43}$	151	158	4.4	6.0
${}_0S_{44}$	149	156	4.4	7.0
${}_0S_{45}$	147	154	4.5	7.0
${}_0S_{46}$	147	152	3.3	7.0
${}_0S_0$	5700	5684	−0.3	5.0
${}_1S_0$	1850	1903	2.8	12.0
${}_3S_0$	1410	1407	−0.2	10.0
${}_4S_0$	1215	1202	−1.1	5.0
${}_5S_0$	1250	1262	0.9	10.0
${}_6S_0$	1150	1276	9.9	17.0
${}_3S_1$	900	867	−3.8	11.0
${}_5S_2$	315	350	9.9	10.0
${}_6S_2$	2900	2257	−28.5	70.0
${}_{10}S_2$	1080	1053	−2.6	10.0
${}_{13}S_2$	1025	1048	2.1	10.0
${}_1S_3$	340	306	−11.0	15.0
${}_2S_3$	541	486	−11.4	18.0
${}_5S_3$	339	324	−4.7	17.0
${}_7S_3$	2800	3565	21.4	60.0
${}_1S_4$	297	295	−0.8	23.0
${}_5S_4$	457	524	12.7	22.0
${}_5S_5$	511	536	4.6	24.0
${}_2S_6$	235	256	8.1	18.0
${}_5S_6$	501	533	6.1	15.0
${}_5S_7$	479	521	8.0	29.0
${}_2S_8$	227	216	−5.1	7.0
${}_2S_{10}$	193	199	3.2	10.0
${}_2S_{12}$	189	192	1.3	15.0

PHILOSOPHICAL TRANSACTIONS OF THE ROYAL SOCIETY A MATHEMATICAL, PHYSICAL & ENGINEERING SCIENCES

models to have a minimum ratio q_μ/q_κ throughout all solid regions or we can assign a different ratio in each layer. Let ρ be the minimum ratio q_μ/q_κ and introduce

$$q_\zeta = q_\mu - \rho q_\kappa. \tag{39}$$

The constraint $q_\zeta \geqslant 0$ in solid regions can be imposed by a simple change of variables in (12) and subsequent equations, including (19). In this way physical constraints, in addition to positivity and monotonicity, can be imposed.

TABLE 7. THE EFFECT ON THE DATA FIT OF CONSTRAINING BULK DISSIPATION TO BE PROPORTIONAL TO SHEAR DISSIPATION

(*a*) Without bulk dissipation in the outer core

ρ	${}_0S_0$ relative misfit	χ (all modes)	χ (radial modes)	ϵ (%)
1	−0.001	6.15	0.98	3.3
10	−0.006	6.54	1.58	3.5
20	−0.008	6.78	2.07	3.6
30	−0.008	6.87	2.24	3.7
40	−0.008	6.93	2.33	3.7
50	0.015	6.97	2.41	3.7
60	0.056	7.10	2.71	3.8
70	0.086	7.26	3.05	3.9
80	0.109	7.41	3.36	4.0

(*b*) With bulk dissipation in the outer core

					Q_κ outer core
1	−0.001	6.14	0.95	3.3	49000
10	−0.004	6.47	1.63	3.5	7200
20	−0.006	6.70	2.11	3.6	6600
50	0.016	6.88	2.46	3.7	6200
80	0.111	7.32	3.41	3.9	5900

Following are the results of some numerical experiments with the 62 observed attenuation data. Using the three-layer mantle model (3484 km, 5700 km, 5959 km, 6371 km), requiring $q_\kappa \equiv 0$ in the outer core, we have used the n.n.l.s. procedure for (19) and (39) for $1 \leqslant \rho \leqslant 80$. The results are summarized in table 7*a*. For $\rho = 1$ the model has q_κ concentrated in the transition zone (5700–5950 km). As ρ increases q_ζ in (39) approaches zero and for large ρq_κ is concentrated in the upper mantle.

Allowing $q_\kappa \geqslant 0$ in the outer core yields the results in table 7*b*. Changing the constraint on q_κ in the outer core leads to very similar results for q_κ in the mantle in the two experiments. The numerical experiments make it plausible that $q_\mu < 80\, q_\kappa$ somewhere in the Earth. Since q_μ is well constrained, in an average way, by the ${}_0S_l$ modes it is better to state the result as $Q_\kappa < 80\, Q_\mu$ somewhere in the Earth. Taking $Q_\kappa \geqslant 50\, Q_\mu$ in the mantle provides an acceptable fit to the 62 observed ${}_nS_l$ attenuation data, including the radial modes whose elastic potential energy is stored primarily in compression. The model for $\rho = 50$ in table 7*a* is shown in figure 23*c*.

We turn next to an analysis of resolving power for the 62 observed data in table 6. In the first analysis we determine average q by using (21)–(31). We consider two regions, the inner core and the mantle. For q_κ in the inner core the minimum spill-over, $1 - \Delta a_j g_j$ (see (27)–(31)) is 0.39 with $\sigma = 19\,\%$. The average q is 1/1580. The large spill-over biases the average by including some q_μ

in the mantle. The actual mean q_κ must be smaller than 1/1580 but we do not have enough s.E.d. to do a better analysis. If we reduce the error the spill-over increases and average q decreases.

The results for q_κ in the mantle and for q_μ in both the inner core and the mantle are summarized in figure 24*a–c*. In each case the best $A(x)$ is shown. We can see that q_κ in the mantle is biased to a high value, 1/2300, by the spill-over of $A(x)$ into regions of large q_μ. Also, q_μ in the inner core is biased to a high value by spill-over of $A(x)$ into regions of mantle q_μ. For q_μ in the mantle the

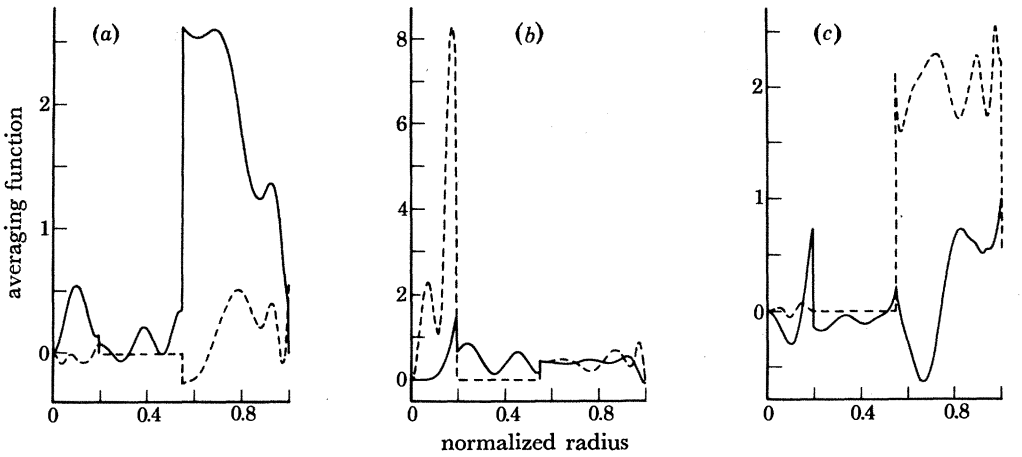

FIGURE 24. Boxcar-like averaging functions constructed from 62 observed data. See the caption to figure 21 for details. Optimum averaging functions are shown for (*a*) q_κ in the mantle ($\bar{q}$ = 1/2300, spill-over = 0.14, σ = 9%); (*b*) q_μ in the inner core ($\bar{q}$ = 1/1000, spill-over = 0.44, σ = 10%); (*c*) q_μ in the mantle ($\bar{q}$ = 1/272, spill-over = 0.08, σ = 4%). The average values for q_κ in the mantle and q_μ in the inner core are biased by the large spill-over of the averaging function into regions of large q_μ.

spill-over is into regions of low attenuation and the large q_μ attenuation in the mantle should be only slightly biased. We must recognize that the area of $A(x)$ for q_μ in the mantle is 0.92 for unimodular $A(x)$. If we rescale $A(x)$ to have unit area in the desired region we must divide mean q by 0.92. This gives mean q = 1/250, and the relative error is unchanged. The mean q is very close to the values belonging to the models, obtained by variations on the n.n.l.s. procedure, shown in figures 22 and 23. Because q in other regions is very likely much smaller than q_μ in the mantle and because the spill-over is small we can adopt 1/250 ($\pm$4%) as a good estimate of mean q_μ in the mantle.

A slight improvement over rescaling $A(x)$ comes from changing the unimodular constraint (29) to the constraint of unit area in the interval being analysed. To do this we impose the constraint

$$\Delta a_j g_j = 1,$$

where Δ and g_j are given by (27). With this constraint we have for (28)

$$\|B(x) - A(x)\|^2 = \mu = a_j a_j - \Delta^{-1}. \tag{40}$$

The calculation becomes, in place of (30),

$$\text{minimize } \mu \cos\theta + wv \sin\theta \text{ subject to } \Delta a_j g_j = 1. \tag{41}$$

The solution for a_j is

$$b_j = g_j/d_j, \quad \lambda = 1/b_j g_j, \quad \text{summation implied}, \quad a_j = \lambda b_j/\Delta \tag{42}$$

where d_j is given in (31). The total area of $A(x)$ is now $a_j h_j$ (see (29)). The area in the interval embraced by Δ is unity. The total area may be either greater or smaller than unity. With constraint (39) we redefine the spill-over to be $a_j h_j - 1$. Positive spill-over indicates net positive area outside the interval and the contrary for negative spill-over. Along the trade-off curve $0 \leqslant \theta \leqslant \frac{1}{2}\pi$, μ is a monotonically increasing function of θ, and ν a monotonically decreasing one, as before.

We return to our analysis of the resolving power of the 62 observed data and continue to seek means of q in the inner core and in the mantle. For q_κ in the inner core the minimum spill-over of 0.20 occurs at $\theta = 0$, but $\sigma = 116\,\%$ there. Reducing σ to 60 % gives a larger spill-over of 0.27 and a mean $q = 1/3000$. This result is qualitatively similar to the previous one with the unimodular constraint.

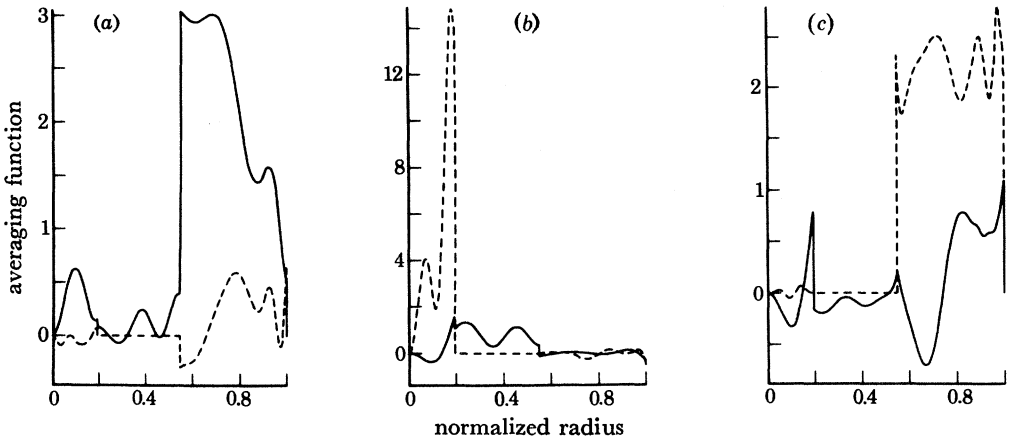

FIGURE 25. Boxcar-like averaging functions with the constraint of unit area in the interval under analysis. The shapes of the functions are very similar to those in figure 24, which were constrained to have unit total area. Optimum averaging functions are shown for (*a*) q_κ in the mantle ($\bar{q} = 1/2200$, spill-over = 0.15, $\sigma = 11\,\%$); (*b*) q_μ in the inner core ($\bar{q} = 1/3500$, spill-over = 0, $\sigma = 61\,\%$); (*c*) q_μ in the mantle ($\bar{q} = 1/250$, spill-over = 0.08, $\sigma = 4\,\%$).

Figures 25*a–c* summarize the results for q_κ in the mantle and q_μ both in the inner core and in the mantle. Changing the constraint is beneficial to the analysis of q_μ in the inner core. The spill-over changes sign along the trade-off curve. At the zero crossing $A(x)$ is shown in figure 25*b*. There is very little bias, and, of course, no spill-over on average. Even though $A(x)$ is not rectangular, if q_μ is nearly constant in the inner core our analysis allows us to infer $q_\mu = 1/3500$ ($\pm 61\,\%$) there.

Changing the constraint from (30) to (41) has given a nearly unbiased estimate of mean q_μ in the mantle with an $A(x)$ that has unit area in the chosen interval. The bias comes from regions of small attenuation and is ignorable at the σ level for the estimate. We conclude the interval analysis of resolving power with the statement that, in the mantle, mean $q_\mu = 1/250$ ($\pm 4\,\%$).

Results for discretized resolving power are presented for the six layers used to define the q_μ model in figure 19*a*. Again we emphasize that the linear averages are independent of the attenuation model used in the computation of the eigenfunctions. Our linear resolving power analysis gives us linear averages of q that are constructed from the data, not from a model derived from the data.

We confine our analysis to q_μ which is taken to be zero in the outer core. Thus the six-layer

model actually has 11, rather than 12, q parameters. The results for each layer are given in table 8*a* at the optimum trade-off between ripple and error. For example, at the base of the mantle (layer 3) the minimum ripple is 0.006, $\sigma = 41\,\%$ and the mean q is 1/510. Increasing the ripple to 0.07 gives $\sigma = 26\,\%$ and a mean q of 1/450. In the inner core the minimum ripple is 0.005, $\sigma = 78\,\%$ and the mean q is 1/4500. Increasing the ripple to 0.04 reduces σ to 40 % and gives a mean q of 1/2600. The bias induced by a non-zero ripple can be assessed by looking at the averaging vector, A_k (see (32)–(38)). This appears to be small as illustrated by the example for layer 1 in table 8*b*.

TABLE 8. RESULTS FROM A DISCRETIZED RESOLVING POWER ANALYSIS OF SHEAR DISSIPATION

(*a*) Results at the optimum trade-off between ripple and error for each layer of a six-shell model

shell radius/km	layer	relative ripple	mean error (%)	q_μ
0–1229	1	0.04	40	1/2600
3484–4107	3	0.07	26	1/450
4107–5458	4	0.016	8.9	1/320
5458–5950	5	0.011	8.7	1/300
5950–6371	6	0.011	2.5	1/117

(*b*) Averaging vector A for q_μ in the inner core; $\sigma = 40\,\%$, ripple is 0.04 and mean $q = 1/2600$

layer	A_κ	A_μ
1	0.013	0.927
2	0.020	0
3	0.006	−0.001
4	0.007	0.008
5	0.004	0.008
6	−0.002	0.008

By asserting that the layer structure in figure 19*a* is an adequate model for our set of 62 data we gain, via discretized resolving power, better resolution than can be obtained otherwise. Simply seeking interval averages permits us to infer less than in the preceding analysis. The interval averages are poorly resolved but are not biased by a preconceived idea of structure. The price we pay for better resolution is the subjective assertion of structure, a price many are willing to bear.

5. DISCUSSION

Our modelling experiments have shown the need to apply constraints to the models to overcome the inherent δ-function structure associated with the non-negativity condition for q. Monotonicity of q_μ in the mantle, with q_μ a non-decreasing function of radius, is compatible with the data and withstands the analysis of discretized resolving power. To learn anything about q_κ, other than it must be positive somewhere, we resort to arguments like those of Heinz *et al.* (1982). Our numerical experiments on ρ, the minimum ratio of q_μ to q_κ (or Q_κ to Q_μ), suggest that $\rho < 80$ somewhere in the Earth's solid regions. The model in figure 23*c* with $\rho = 50$ in solid regions is compatible with the data. Choosing $\rho = 50$ forces q_κ to be concentrated in the upper mantle. From these results we see that the incorporation of plausible physical constraints into the modelling procedure leads to a subset of models whose features vary little from one model to another. If the physical constraints are not only plausible but also close to the truth, then the subset of acceptable models should be close to the Earth. For convenience, we list the parameters of the model in figure 23*c* in table 9*a* and show the fit to the observed data in table 9*b*.

If our observations of the two core modes ${}_6S_2$ and ${}_7S_3$ are not seriously wrong then the inner core must have a low q_μ. Simply to have the core modes observable places this requirement on the inner core, at least at the low frequencies considered in this paper. The elastic properties of the inner core are consistent with those of a normal solid (Falzone & Stacey 1980) so $q_\kappa < q_\mu$ there and probably $q_\kappa \ll q_\mu$ there.

Modes that are PKIKP equivalent, e.g. ${}_{10}S_2$, ${}_{13}S_2$, require q_μ in the inner core to be small ($< 1/1000$) independently of the core mode observations, and prevent model q_κ in the outer core from rising above about 1/6000. (We note that $q_\kappa = 0$ in the outer core is compatible with the data.) Consequently, for smooth models of q_μ and for $q_\kappa \ll q_\mu$ in the mantle it is reasonable that q_κ is concentrated in the upper mantle. It must be emphasized that it is a combination of the data and the physical constraint $q_\mu \geqslant \rho q_\kappa$, with $\rho = 50$ giving a good fit to the data, that forces the localization of bulk attenuation into the upper mantle.

Overall, our linear resolving power analysis shows $q_\mu = 1/3500 \pm 61\,\%$ in the inner core and $q_\mu = 1/250 \pm 4\,\%$ in the mantle. By comparison Sailor & Dziewonski (1978) have $q_\mu = 1/256$ in the mantle of their model QBS and $q_\mu = 1/252$ for model QKB. The similarity between their result and ours is clear; yet it is important to realize that our result is independent of any particular model of attenuation, a salient feature of all linear inverse problem. The resolving power analysis shows that we do not have enough s.E.d. of the right kind to resolve q_κ in the absence of constraints or to resolve q_μ in smaller intervals.

The average q_μ in the mantle belongs to the frequency band below 5 mHz and is centred at, say, 3 mHz. At higher frequencies the work of Sipkin & Jordan (1980) using multiple ScS pulses gives a mantle average $q_{ScS} = 1/170 \pm 20\,\%$ in a frequency band centred at, say, 30 mHz. To relate q_{ScS} to q_μ in the mantle we must account for the effect of shear velocity. The ScS pulse travels more slowly in the high attenuation zones of the upper mantle and more swiftly in the lower attenuation zones of the lower mantle. Consequently, $q_{ScS} > q_\mu$. The ratio q_{ScS}/q_μ is dependent on the distribution of shear velocity. For a large class of Earth models the ratio is very close to 1.1. Thus, our q_μ of 1/250 implies a q_{ScS} of 1/227. Sipkin & Jordan (1979) have discussed the frequency dependence of q_{ScS} in considerable detail. Our result for low frequencies is in agreement with their findings. These two, independent results argue strongly for the variation of q_μ with frequency. If the frequency dependence of q can be better constrained then some insight into the physical mechanisms of attenuation will be gained; however, the present low frequency data are clearly inadequate for this purpose.

Many kinds of seismological data are very redundant in that the span of their data functions is far less than their number. In this paper we have shown that attenuation data are no exception. In the example with synthetic data there are 200 gross Earth data (g.E.d.) each with an assigned relative standard deviation of 1 %, but they have only 22 significant Earth data (s.E.d.) with relative standard deviations less than 10 %. For our set of observed attenuation data there are 71 g.E.d., 62 after rejection of outliers, but they have only 5 s.E.d. with relative standard deviations less than 10 %. These 5 s.E.d. come from an analysis of 557 IDA records, 2 South Pole records and 1 record of the Colombian event (31 July 1970). Each of the 560 records has been analysed for about 50 modes on the average. The outcome is 5 s.E.d. Clearly, if we are to learn more about the distribution of attenuation in the Earth we must increase the number of s.E.d. by an order of magnitude, to 50 or 100 s.E.d. Meeting this requirement means that many more observations of attenuation must be made.

It may be possible to make some more progress in the analysis of individual records. Records

TABLE 9. A SIMPLE Q MODEL WITH BULK Q CONSTRAINED TO BE AT LEAST 50 × SHEAR Q

(*a*) Model parameters

shell radius/km	shear Q	bulk Q
0–1229	3666	183300
3484–5700	304	15210
5700–5950	264	13180
5950–6371	118	5898

(*b*) Comparison of the data predicted by the model with the observations

mode	observed Q	model Q	difference (%)	s.d. (%)
${}_0S_4$	391	371	−5.3	23.0
${}_0S_7$	345	334	−3.2	7.0
${}_0S_8$	356	328	−8.5	7.0
${}_0S_9$	340	323	−5.2	4.0
${}_0S_{10}$	328	320	−2.6	5.0
${}_0S_{12}$	311	314	0.9	4.0
${}_0S_{13}$	321	311	−3.3	3.0
${}_0S_{14}$	294	307	4.1	3.0
${}_0S_{15}$	318	302	−5.4	3.0
${}_0S_{16}$	287	296	3.0	2.0
${}_0S_{17}$	269	289	7.1	3.0
${}_0S_{20}$	254	267	5.0	4.0
${}_0S_{21}$	263	260	−1.3	2.0
${}_0S_{22}$	253	252	−0.5	3.0
${}_0S_{23}$	248	244	−1.5	2.0
${}_0S_{24}$	247	237	−4.2	4.0
${}_0S_{25}$	225	230	2.2	4.0
${}_0S_{26}$	227	224	−1.5	3.0
${}_0S_{27}$	219	218	−0.7	3.0
${}_0S_{28}$	212	212	−0.1	3.0
${}_0S_{29}$	213	206	−3.2	3.0
${}_0S_{30}$	207	201	−2.8	4.0
${}_0S_{31}$	197	197	−0.2	4.0
${}_0S_{32}$	199	192	−3.5	4.0
${}_0S_{33}$	179	188	4.9	3.0
${}_0S_{34}$	182	185	1.4	4.0
${}_0S_{35}$	175	181	3.4	4.0
${}_0S_{36}$	179	178	−0.6	3.0
${}_0S_{37}$	179	175	−2.3	3.0
${}_0S_{38}$	176	172	−2.3	2.0
${}_0S_{39}$	163	170	3.9	5.0
${}_0S_{40}$	162	167	3.1	5.0
${}_0S_{41}$	162	165	1.8	4.0
${}_0S_{42}$	164	163	−0.7	8.0
${}_0S_{43}$	151	161	6.2	6.0
${}_0S_{44}$	149	159	6.4	7.0
${}_0S_{45}$	147	157	6.7	7.0
${}_0S_{46}$	147	156	5.7	7.0
${}_0S_0$	5700	5784	1.5	5.0
${}_1S_0$	1850	1824	−1.4	12.0
${}_3S_0$	1410	1520	7.2	10.0
${}_4S_0$	1215	1361	10.7	5.0
${}_5S_0$	1250	1288	3.0	10.0
${}_6S_0$	1150	1308	12.1	17.0
${}_3S_1$	900	854	−5.4	11.0
${}_5S_2$	315	353	10.7	10.0
${}_6S_2$	2900	1976	−46.8	70.0
${}_{10}S_2$	1080	1169	7.6	10.0

PHILOSOPHICAL TRANSACTIONS OF THE ROYAL SOCIETY A MATHEMATICAL, PHYSICAL & ENGINEERING SCIENCES

TABLE 9. (*cont.*)

(*b*) Comparison of the data predicted by the model with the observations

mode	observed Q	model Q	difference (%)	s.d. (%)
${}_{13}S_2$	1025	1187	13.6	10.0
${}_{1}S_3$	340	296	−14.7	15.0
${}_{2}S_3$	541	455	−19.0	18.0
${}_{5}S_3$	339	316	−7.2	17.0
${}_{7}S_3$	2800	2842	1.5	60.0
${}_{1}S_4$	297	286	−3.9	23.0
${}_{5}S_4$	457	521	12.3	22.0
${}_{5}S_5$	511	539	5.2	24.0
${}_{2}S_6$	235	256	8.1	18.0
${}_{5}S_6$	501	544	7.9	15.0
${}_{5}S_7$	479	527	9.2	29.0
${}_{2}S_8$	227	217	−4.6	7.0
${}_{2}S_{10}$	193	200	3.4	10.0
${}_{2}S_{12}$	189	190	0.8	15.0

$\epsilon = 3.7\%$
$\chi = 6.97$

from the Global Digital Seismic Network may enable us to analyse ${}_0T_l$ modes on horizontal components just as we have done for ${}_0S_l$ modes on vertical components in this paper. For a given angular order l the fundamental toroidal mode has its shear energy density more strongly concentrated toward the surface than the fundamental spheroidal mode. Numerous, accurate ${}_0T_l$ data should improve the resolution of q_μ in the upper mantle. Some extension of the analysis of single records to overtones has been reported in this paper. More observations are desirable and may come from the horizontal components, but the increase in data will be limited. Overtones are more difficult to analyse than fundamental modes because they are usually less well excited. Also, for weakly attenuated overtones, such as core modes and PKIKP equivalent modes, the effect of very slight splitting can be severe. What is really needed is the observation of singlets.

Recent progress in determining the large-scale, aspherical structure (Masters *et al.* 1982; Dziewonski *et al.* 1977) suggests we can calculate the geographical shapes of singlets for realistic, three-dimensional models. The geographical shapes are necessary for use in multiple-record analyses, such as stacking. Some variation on the theme of stacking appears to be the indicated method for multiple record analysis. Only in this way can a large number of singlets be measured and the number of s.E.d. increased tenfold or more.

The research in this report was supported by the U.S. National Science Foundation under grant EAR-79-23779. We thank Dr Jon Berger and Dr Duncan Agnew for providing the very high quality IDA data, Professor Leon Knopoff for the two records from the South Pole and Dr William Farrell for the record of the deep-focus Colombian event. Discussions with Professor Robert Parker about constrained optimization and with Professor Thomas Jordan about the frequency dependence of q_μ and q_{ScS} were very useful. Mrs Elaine Blackmore patiently and expertly prepared the manuscript. Mrs Ruth Zdvorak was very helpful in the preparation of the figures.

PHILOSOPHICAL TRANSACTIONS OF THE ROYAL SOCIETY A MATHEMATICAL, PHYSICAL & ENGINEERING SCIENCES

Appendix A. A least-squares algorithm for estimating modal properties

The expression for the recorded vertical acceleration of a single mode of oscillation of angular order l is given by (Gilbert 1980)

$$a_k(\boldsymbol{r}, t) = A_k(\boldsymbol{r}, \boldsymbol{r}_0, t)^* [C_k(t) - d_k H(t)], \tag{A 1}$$

where

$$C_k = [\cos(\omega_k t - \phi_k)/\cos\phi_k]\, \mathrm{e}^{-\alpha_k t}, \tag{A 2}$$

$$d_k = S_k(r)/AU_k(r),$$

$$\tan\phi_k = [-\alpha_k\omega_k U_k(r) + \alpha_k\omega_k^{-1} S_k(r)]/AU_k(r),$$

$$S_k(r) = 2r^{-1} g(r)\, U_K(r) + (l+1)\, r^{-1}\Phi_k(r),$$

$$AU_k(r) = \omega_k^2 U_k(r) + S_k(r).$$

In (A 1) A_k is the amplitude of the kth mode; $\sigma_k\ (=\omega_k + \mathrm{i}\alpha_k)$ is the complex frequency and it is assumed that $\alpha_k \ll \omega_k$. The scalar U is the displacement scalar and Φ is the scalar for the perturbations in the gravitational potential. The function $C_k(t)$ is the resonance function for unit acceleration and d_k is the residual acceleration for a step function source. It is caused by the redistribution of mass (giving Φ a static value) and by the static displacement. In the practical analysis of low frequency data, it is convenient to remove the Earth tides and the static response by a process of least-squares fitting prior to the estimation of modal properties. The fitting of resonance peaks is done in the frequency domain so the Fourier transform of (A 1) is taken:

$$a_k(\boldsymbol{r}, \omega) = A_k(\boldsymbol{r})\, C_k(\omega). \tag{A 3}$$

The frequency dependence of the amplitude is ignored as the spectrum of the source is likely to be smooth and may be assumed to be constant across a spectral peak. If there are N resonance peaks that are sufficiently close together in a given frequency band to require simultaneous estimation then the observed spectrum is simply a sum of modes (A 3),

$$F(\boldsymbol{r}, \omega) = \sum_{k=1}^{N} A_k(\boldsymbol{r})\, C_k(\omega),$$

or, in matrix notation

$$\boldsymbol{F} = \boldsymbol{C}\cdot\boldsymbol{A}. \tag{A 4}$$

$\boldsymbol{C}$ is a matrix of singlet spectra evaluated at an arbitrary number of points across each peak. $\boldsymbol{A}$ is an array of the complex amplitudes of the modes in the band and $\boldsymbol{F}$ is the observed spectrum. $\boldsymbol{C}$ depends on $2N$ unknown variables, p_j say, where $p_1 = \omega_1$, $p_2 = \alpha_1$, $p_3 = \omega_2$ and so on. Given initial estimates of the complex frequencies, $\boldsymbol{C}_0$ may be evaluated (the zero subscript refers to our initial guess of the p_j). Performing the minimization

$$\min\,(\boldsymbol{C}_0\cdot\boldsymbol{A} - \boldsymbol{F})$$

by least-squares gives an initial estimate of the complex amplitudes, $\boldsymbol{A}_0$. To refine our estimates of $\boldsymbol{p}$ we linearize the dependence of the spectrum on $\boldsymbol{p}$, i.e.

$$\delta\boldsymbol{F} = \boldsymbol{C}_0\cdot\delta\boldsymbol{A} + \boldsymbol{D}\cdot\boldsymbol{A}_0\delta\boldsymbol{p} \tag{A 5}$$

where $\boldsymbol{D}$ is a matrix of partial derivatives of $\boldsymbol{C}_0$ with respect to the $\boldsymbol{p}$. In general the perturbations in amplitude and $\boldsymbol{p}$ are coupled but, because amplitude is linearly related to the spectrum, we

can decouple the perturbations to first order in $\delta \boldsymbol{p}$. We use the SVD (Wilkinson & Reinsch 1971) representation of $\boldsymbol{C}_0$,

$$\boldsymbol{C}_0 = \boldsymbol{U}\boldsymbol{\Lambda}\boldsymbol{V}^{\mathrm{T}}, \quad \boldsymbol{\Lambda} = \mathrm{diag}\{\lambda_1, \lambda_2, \ldots\}, \tag{A 6}$$

and write the least-squares solution

$$\boldsymbol{A}_0 = \boldsymbol{V}\boldsymbol{\Lambda}^{-1}\boldsymbol{U}^{\mathrm{T}}\boldsymbol{F}. \tag{A 7}$$

The residual $\delta \boldsymbol{F}$ in (A 5) is then

$$\delta \boldsymbol{F} = \boldsymbol{F} - \boldsymbol{C}_0 \boldsymbol{A}_0 = (\boldsymbol{I} - \boldsymbol{U}\boldsymbol{U}^{\mathrm{T}})\,\boldsymbol{F}. \tag{A 8}$$

We recognize $\boldsymbol{I} - \boldsymbol{U}\boldsymbol{U}^{\mathrm{T}}$ in (A 8) as the projection matrix that projects $\boldsymbol{F}$ into the residual space. Solving (A 5) for $\delta \boldsymbol{A}$ and using (A 6) and (A 7) we have

$$\delta \boldsymbol{A} = \boldsymbol{V}\boldsymbol{\Lambda}^{-1}\boldsymbol{U}^{\mathrm{T}}(\delta \boldsymbol{F} - \boldsymbol{D}\cdot\boldsymbol{A}_0\,\delta \boldsymbol{p}). \tag{A 9}$$

Although $\boldsymbol{U}\boldsymbol{U}^{\mathrm{T}} \neq \boldsymbol{I}$ in data space, $\boldsymbol{U}^{\mathrm{T}}\boldsymbol{U} = \boldsymbol{I}$ in parameter space, so the first term on the right-hand side of (A 9) vanishes and we have a linear relation between $\delta \boldsymbol{A}$ and $\delta \boldsymbol{p}$:

$$\delta \boldsymbol{A} = -\boldsymbol{V}\boldsymbol{\Lambda}^{-1}\boldsymbol{U}^{\mathrm{T}}\boldsymbol{D}\cdot\boldsymbol{A}_0\,\delta \boldsymbol{p}. \tag{A 10}$$

In (A 10) the square matrix $-\boldsymbol{V}\boldsymbol{\Lambda}^{-1}\boldsymbol{U}^{\mathrm{T}}\boldsymbol{D}\cdot\boldsymbol{A}_0$ is the partial derivative of $\boldsymbol{A}$ with respect to $\boldsymbol{p}$. Its use decouples the determination of $\delta \boldsymbol{A}$ and $\delta \boldsymbol{p}$. This is seen by combining (A 5) and (A 10) to obtain

$$[(\boldsymbol{I} - \boldsymbol{U}\boldsymbol{U}^{\mathrm{T}})\,\boldsymbol{D}\cdot\boldsymbol{A}_0]\,\delta \boldsymbol{p} = \delta \boldsymbol{F}. \tag{A 11}$$

Solving (A 11) for $\delta \boldsymbol{p}$ allows us to recompute $\boldsymbol{C}$ and to reapply (A 6)–(A 11). The convergence of this iterative procedure is usually very fast and is stabilized numerically by the use of (A 10). Choosing too many parameters (too many modes) retards the convergence of the procedure and leads to the trade-offs discussed in § 2.

Although the projection matrix $\boldsymbol{I} - \boldsymbol{U}\boldsymbol{U}^{\mathrm{T}}$ is always singular, the columns of $\boldsymbol{U}$ span its null space, we see that to prevent $\boldsymbol{I} - \boldsymbol{U}\boldsymbol{U}^{\mathrm{T}}$ from vanishing identically we must have more data than parameters. If they are equal in number then $\boldsymbol{U}\boldsymbol{U}^{\mathrm{T}} = \boldsymbol{I}$ and the vanishing of (A 11) shows that an exact fit to the data can be made with effectively any choice of parameters followed by the solution of (A 4) for $\boldsymbol{A}$. In practice we have found that 3–5 complex frequency points per mode, clustered in a band $3\alpha_k$ wide about the apparent centre frequency, make (A 11) numerically stable.

In general the data are not perfect and have a panel structure. The panels of bad data are due to nonlinear instrumental effects during the passage of very high amplitude surface waves, aftershocks, etc. They are zero in-filled and we introduce the panel structure $P(t)$, which is unity in panels of good data and zero elsewhere. Equation (A 2) must therefore be modified:

$$C_k(t) = P(t)\,[\cos(\omega_k t - \phi)/\cos\phi]\,\mathrm{e}^{-\alpha_k t}. \tag{A 12}$$

The derivatives with respect to α_k and ω_k are

$$\frac{\partial C_k(t)}{\partial \alpha_k} = -\frac{tP(t)}{\cos\phi}\cos(\omega_k t - \phi)\,\mathrm{e}^{-\alpha_k t}, \quad \frac{\partial C_k(t)}{\partial \omega_k} = -\frac{tP(t)}{\cos\phi}\sin(\omega_k t - \phi)\,\mathrm{e}^{-\alpha_k t}. \tag{A 13}$$

When a taper is applied (A 12) and (A 13) must be multiplied by the taper function. The matrix $\boldsymbol{C}$ is composed of the Fourier transform of (A 12) evaluated at an arbitrary number of points across the peak. For any reasonable taper the matrix elements can be evaluated semi-analytically. The same is true of the matrix $\boldsymbol{D}$, which is composed of the Fourier transform of (A 13) evaluated

at the same frequency points. Furthermore, if the frequency band is narrow, i.e. if $|\omega - \omega_k| \ll \omega$, then to a very good approximation

$$\frac{\partial C_k}{\partial \omega_k}(\omega) = -\mathrm{i}\frac{\partial C_k}{\partial \alpha_k}(\omega). \tag{A 14}$$

The fact that both $\boldsymbol{C}$ and $\boldsymbol{D}$ can be rapidly calculated makes this method extremely fast. Indeed, the slowest part of the algorithm is the evaluation of the Fourier transform of the data. Because we are usually concerned with fitting a few frequency points about a resonance peak it is more efficient to use Goertzel's algorithm than to use an f.F.t. The original Goertzel algorithm suffers from round-off errors at low and high frequencies and modified recursion formulae must be used to retain accuracy throughout the spectrum (Gentleman 1969).

Appendix B. Project IDA stations

location	code	latitude	longitude	elevation m	period of operation (month/year)
Brasília, Brazil	BDF	15° 39′ 50″ S	47° 54′ 12″ W	1260	4/77–
Canberra, Australia	CAN	35° 19′ 15″ S	148° 59′ 55″ E	650	1/75–4/78
College, Alaska, U.S.A.	CMO	64° 51′ 36″ N	147° 50′ 06″ W	183	7/77–
Easter Island, Chile	EIC	27° 09′ 29″ S	109° 26′ 04″ W	42	8/78–
Erimo, Japan	ERM	42° 00′ 54″ N	143° 09′ 26″ E	40	8/80–
Eskdalemuir, Scotland, U.K.	ESK	55° 19′ 00″ N	3° 12′ 18″ W	242	9/78–
Garm, U.S.S.R.	GAR	39° 00′ 00″ N	70° 19′ 00″ E	1300	9/76–12/80
Guam, Mariana Is.	GUA†	13° 32′ 18″ N	144° 54′ 42″ E	230	7/79–
Halifax, N.S., Canada	HAL	44° 38′ 16″ N	63° 35′ 30″ W	38	4/76–
Kipapa, Hawaii, U.S.A.	KIP	21° 25′ 24″ N	158° 00′ 54″ W	70	9/77–
Kunming, China	KMY	25° 08′ 54″ N	102° 44′ 49″ E	1952	10/80–
Naña, Peru	NNA	11° 59′ 15″ S	76° 50′ 32″ W	575	6/75–
Piñon Flat, Calif., U.S.A.	PFO	33° 36′ 33″ N	116° 27′ 19″ W	1280	2/76–
Rarotonga, Cook Islands	RAR	21° 12′ 45″ S	159° 46′ 24″ W	28	10/76–
Mahé, Seychelles	SEY‡	4° 36′ 54″ S	55° 29′ 27″ E	270	1/80–
South Pole, Antarctica	SPA§	90° 00′ 00″ S	—	2927	1/79–
Saint-Sauveur, France	SSB	45° 16′ 45″ N	4° 32′ 31″ E	700	9/81–
Sutherland, S. Africa	SUR	32° 22′ 47″ S	20° 48′ 04″ E	1770	12/75–
Adelaide, Australia	TWO	35° 01′ 57″ S	138° 34′ 41″ E	165	4/78–

† From 7/79 through 10/79 this station was located at 13° 35′ 18″ N, 144° 51′ 42″ E.
‡ From 1/80 through 10/80 this station was located at 4° 40′ S, 55° 29′ E.
§ Instrument installed and operated by U.C.L.A.; the date given here is the time at which an IDA filter and recorder were added.

References

Aki, K. & Richards, P. G. 1980 *Quantitative seismology*. San Francisco: W. H. Freeman.

Anderson, D. L. & Hart, R. S. 1978 *Q* of the Earth. *J. geophys. Res.* **83**, 5869–5882.

Backus, G. & Gilbert, F. 1967 Numerical applications of a formalism for geophysical inverse problems. *Geophys. Jl R. astr. Soc.* **13**, 247–276.

Backus, G. & Gilbert, F. 1968 The resolving power of gross Earth data. *Geophys. Jl R. astr. Soc.* **16**, 169–205.

Backus, G. & Gilbert, F. 1970 Uniqueness in the inversion of inaccurate gross Earth data. *Phil. Trans. R. Soc. Lond.* A **266**, 123–192.

Bolt, B. A. & Brillinger, D. R. 1979 Estimation of uncertainties in eigenspectral estimates from decaying geophysical time series. *Geophys. Jl R. astr. Soc.* **59**, 593–603.

Buland, R., Berger, J. & Gilbert, F. 1979 Observations from the IDA network of attenuation and splitting during a recent earthquake. *Nature, Lond.* **277**, 358–362.

Buland, R. & Gilbert, F. 1978 Improved resolution of complex eigenfrequencies in analytically continued seismic spectra. *Geophys. Jl R. astr. Soc.* **52**, 457–470.

PHILOSOPHICAL TRANSACTIONS OF THE ROYAL SOCIETY A MATHEMATICAL, PHYSICAL & ENGINEERING SCIENCES

Chao, B. F. 1981 Symmetry, excitation and estimation in terrestrial spectroscopy. Ph.D. thesis, University of California, San Diego.
Chao, B. F. & Gilbert, F. 1980 Autoregressive estimation of complex eigenfrequencies in low frequency seismic spectra. *Geophys. Jl R. astr. Soc.* **63**, 641–657.
Dahlen, F. A. 1976 Models of the lateral heterogeneity of the Earth consistent with eigenfrequency splitting data. *Geophys. Jl R. astr. Soc.* **44**, 77–105.
Dahlen, F. A. 1979 The spectra of unresolved split normal mode multiplets. *Geophys. Jl R. astr. Soc.* **58**, 1–33.
Dahlen, F. A. 1981 The free oscillations of an anelastic aspherical Earth. *Geophys. Jl R. astr. Soc.* **66**, 1–22.
Dahlen, F. A. 1982 The effect of data windows on the estimation of free oscillation parameters. *Geophys. Jl R. astr. Soc.* **69**, 537–549.
Dratler, J., Farrell, W., Block, B. & Gilbert, F. 1971 High-Q overtone modes of the Earth. *Geophys. Jl R. astr. Soc.* **23**, 399–410.
Dziewonski, A. M. & Anderson, D. L. 1981 Preliminary reference Earth model. *Phys. Earth planet. Int.* **25**, 297–356.
Dziewonski, A. M., Hager, B. H. & O'Connell, R. J. 1977 Large-scale heterogeneities in the lower mantle. *J. geophys. Res.* **82**, 239–255.
Dziewonski, A. M. & Steim, J. 1982 Dispersion and attenuation of mantle waves through wave-form inversion. *Geophys. Jl R. astr. Soc.* **70**, 503–527.
Emmerman, S. & Dahlen, F. A. 1979 Estimating the decay rate of a decaying sinusoid in noise. *EOS* **60**, 324 (abstract).
Falzone, A. J. & Stacey, F. D. 1980 Second-order elastic theory: explanation for the high Poisson's ratio of the inner core. *Phys. Earth planet. Int.* **21**, 371–377.
Geller, R. J. & Stein, S. 1979 Time domain attenuation measurements for fundamental spheroidal modes ($_0S_6$–$_0S_{28}$) for the 1977 Indonesian earthquake. *Bull. seism. Soc. Am.* **69**, 1671–1692.
Gentleman, W. M. 1969 An error analysis of Goertzel's (Watt's) method for computing Fourier coefficients. *Computer J.* **12**, 160–165.
Gilbert, F. 1971 Ranking and winnowing gross Earth data for inversion and resolution. *Geophys. Jl R. astr. Soc.* **23**, 123–128.
Gilbert, F. & Dziewonski, A. 1975 An application of normal mode theory to the retrieval of structural parameters and source mechanisms from seismic spectra. *Phil. Trans. R. Soc. Lond.* A **278**, 187–269.
Hansen, R. A. 1982*a* Simultaneous estimation of terrestrial eigenvibrations. *Geophys. Jl R. astr. Soc.* **70**, 155–172.
Hansen, R. A. 1982*b* Observational study of terrestrial eigenvibrations. *Phys. Earth planet. Int.* **28**, 27–69.
Harris, F. 1978 On the use of windows for harmonic analysis with the discrete Fourier transform. *Proc. Instn. elect. Engrs.* **66**, 51–83.
Heinz, D., Jeanloz, R. & O'Connell, R. J. 1982 Bulk attenuation in a polycrystalline Earth. *J. geophys. Res.* **87**, 7772–7778.
Jordan, T. H. 1978 A procedure for estimating lateral variations from low frequency eigenspectra data. *Geophys. Jl R. astr. Soc.* **52**, 441–455.
Knopoff, L., Zurn, W., Rydelek, P. A. & Yogi, T. 1979 Q of mode $_0S_0$. *J. Geophys.* **46**, 89–95.
Lapwood, E. R. & Usami, T. 1981 *Free oscillations of the earth.* New York: Cambridge University Press.
Lawson, C. L. & Hanson, R. J. 1974 *Solving least squares problems.* Englewood Cliffs, New Jersey: Prentice Hall.
Luenberger, D. G. 1973 *Introduction to linear and nonlinear programming.* Reading, Massachusetts: Addison Wesley.
Luh, P. C. 1974 The normal modes of the rotating, self-gravitating, inhomogeneous Earth. *Geophys. Jl R. astr. Soc.* **38**, 187–224.
Masters, T. G. & Gilbert, F. 1981 Structure of the inner core inferred from observations of its spheroidal shear modes. *Geophys. Res. Lett.* **8**, 569–571.
Masters, G., Jordan, T. H., Silver, P. G. & Gilbert, F. 1982 Aspherical Earth structure from fundamental spheroidal mode data. *Nature, Lond.* **298**, 609–613.
Parker, R. L. 1980 The inverse problem of electromagnetic induction: Existence and construction of solutions based upon incomplete data. *J. geophys. Res.* **85**, 4421–4428.
Riedesel, M., Agnew, D., Berger, J. & Gilbert, F. 1980 Stacking for the frequencies and Q's of $_0S_0$ and $_1S_0$. *Geophys. Jl R. astr. Soc.* **62**, 457–471.
Riedesel, M., Jordan, T. H. & Masters, G. 1981 Observed effects of lateral heterogeneity on fundamental spheroidal modes. *EOS* **62**, 332 (abstract).
Sabatier, P. C. 1977 Positivity constraints in linear inverse problems. I. General theory. *Geophys. Jl R. astr. Soc.* **48**, 415–442.
Sailor, R. V. & Dziewonski, A. M. 1978 Measurements and interpretation of normal mode attenuation. *Geophys. Jl R. astr. Soc.* **53**, 559–582.
Silver, P. G. & Jordan, T. H. 1981 Fundamental spheroidal mode observations of aspherical heterogeneity. *Geophys. Jl R. astr. Soc.* **64**, 605–634.
Sipkin, S. A. & Jordan, T. H. 1979 Frequency dependence of Q_{ScS}. *Bull. seism. Soc. Am.* **69**, 1055–1079.
Sipkin, S. A. & Jordan, T. H. 1980 Regional variation of Q_{ScS}. *Bull. seism. Soc. Am.* **70**, 1071–1102.
Smith, S. W. 1972 The anelasticity of the mantle. *Tectonophys.* **13**, 601–622.

PHILOSOPHICAL TRANSACTIONS OF THE ROYAL SOCIETY A MATHEMATICAL, PHYSICAL & ENGINEERING SCIENCES

Stein, S. & Nunn, J. A. 1981 Analysis of split normal modes for the 1977 Indonesian earthquake. *Bull. seism. Soc. Am.* **71**, 1031–1048.

Wilkinson, J. H. & Reinsch, C. 1971 *Linear algebra*, p. 134–151. Berlin, Heidelberg, New York: Springer Verlag.

Woodhouse, J. H. 1980 The coupling and attenuation of nearly resonant multiplets in the Earth's free oscillation spectrum. *Geophys. Jl R. astr. Soc.* **61**, 261–283.

Xu, G.-M. & Knopoff, L. 1980 Attenuation induced systematic errors in observations of the free mode spectrum. *EOS* **61** (abstract).

PHILOSOPHICAL TRANSACTIONS OF THE ROYAL SOCIETY A MATHEMATICAL, PHYSICAL & ENGINEERING SCIENCES